View metadata, citation and similar papers at core.ac.uk

brought to you by CORE

provided by UPCommons. Portal del coneixement obert de la UPC

DETECTION AND QUANTIFICATION OF SOFT PLAQUE IN CORONARY ARTERIES FROM MSCT IMAGES

by

Eduard Seseras Mas
Advisor: Yongyi Yang

Electrical & Computer Engineering

Illinois Institute of Technology

Chicago, Illinois September 2008

ABSTRACT

Medical research since the early to mid-1990s has indicated that the artery lesion known as soft plaque causes most heart attacks. The recent advances in temporal and spatial resolution of Multi-Slice Computed Tomography (MSCT) allow studying these structures in 3D with high accuracy. This thesis presents a semi-automatic method that detects the soft plaques in the coronary arteries and quantifies their volume from 3D MSCT datasets with limited user interaction. The presented method consists of: (1) the extraction of the artery centerline with an implementation of a multi-scale tracking algorithm, (2) a first segmentation of the vessel's lumen to fix the initial centerline, (3) a final segmentation of the lumen and the wall of the artery, (4) the analysis of the volume along the vessel to detect soft plaques, and (4) the quantification of the plaques volume. The method was evaluated with 3D real medical images..

KEYWORDS

Medical Imaging, Multi-Slice CT, Multi-scale Tracking Algorithm, EM with Gaussian Mixture Model segmentation, Soft Plaque Detection, Volume Quantification, Coronary Arteries.

TABLE OF CONTENTS

ACKNOWLEDGEMENTS

This work that follows would have never been possible without the sincere contribution of a lot of people, starting with Professor Yongyi Yang, who has been the advisor of my work and has been always supporting me with his enthusiasm to keep on trying new solutions. Felix Renard and his appreciated and uninterested help from France has been pivotal in my research as well.

My stay in the MIRC department of the Illinois Institute of Technology could not have been possible without the work of Dr. Vanita Misquita and the initial help of Dr. Jovan Brankov. I honestly thank my colleagues Keivan Majidi, Thibault Marin, Xiaofeng Niu and Xiping Wang to create a pleasant environment in the office with their friendliness.

Finally, I would like to give special thanks to my family, my girlfriend and my Spanish mates in the IIT who were always encouraging me.

GLOSSARY

Atheroma: Abnormal inflammatory accumulation of macrophage white blood cells within the walls of arteries

CAD: Coronary Artery Disease. See section 2.1.

Calcium Score: A number reflecting the degree and extent of calcium deposits in the coronary arteries.

Coronary arteries: Arteries that supply blood to the heart.

EM: Estimation Maximization method. See section 3.3.

GMM: Gaussian Mixture Model

IVUS: Intravascular ultrasound

Lumen: Interior of a vessel within the body.

MI: Myocardial Infarction (heart attack). See section 2.1.

MRI: Magnetic Resonance Imaging.

MSCT: Multi-Slice Computed Tomography. See section 2.2.3.

Soft plaque: An atheroma particularly prone to plaque rupture, which may produce heart attacks. See section 2.1.

Stenosis: Abnormal narrowing in a blood vessel.

Vulnerable plaque: Soft plaque.

Figures

Tables

INTRODUCTION

Heart disease is the leading cause of death in the United States, killing 696,947 people in 2002 [1]. Nevertheless, the scope of the disease and its effects are worldwide. According to a new international health study from the European Heart Journal, heart disease is the primary and most widespread health problem facing countries in Europe [2].

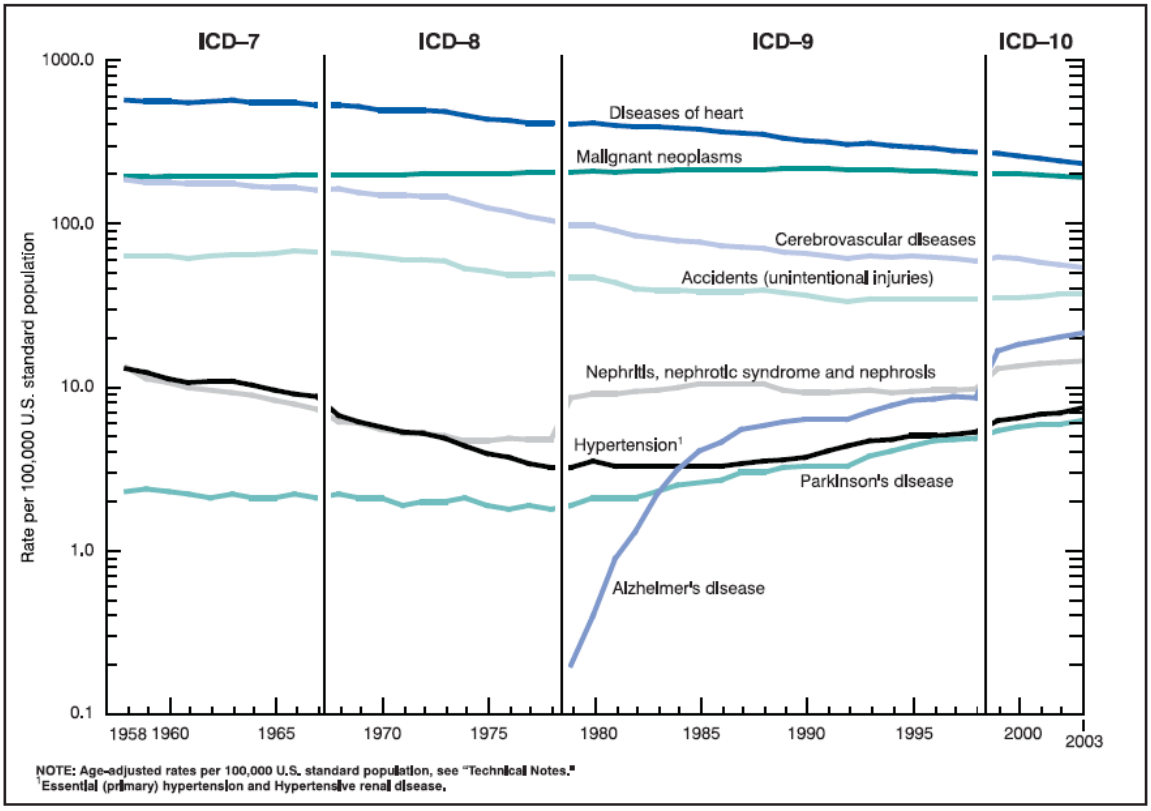

Figure 1: Death reasons in USA from 1958 to 2003. Source: Anderson, Robert N. et al. Deaths: Leading Causes for 2002. National Vital Statistics Reports, 2005.

Despite progress in the understanding of atherosclerosis and coronary artery disease (CAD), main characters in heart disease, about half of all acute myocardial infarctions (MIs) still occur unexpectedly. Moreover, about one-third of people who experience a MI die within 24 hours. Certainly, there is a tremendous need for improving individual patient risk assessment for acute coronary syndromes (ACS).

There is increasing interest in detection of soft plaques in the arteries' walls for the assessment of carotid atherosclerotic disease, as it has revealed to be a predictor of the MI's risk. An automatic detection of these plaques would be useful in the study of their clinical significance.

Recent improvements in the high-resolution Multi-Slice Computed Tomography (MSCT) provide information about the arterial wall that is unavailable with most other non-invasive methods, including angiography. Evidence suggests that this technology, in a future, will be useful in the characterization of plaque composition and microanatomy, thus leading to the identification of lesions that are vulnerable to rupture or erosion.

The Medical Image Research Center of the Illinois Institute of Technology, in collaboration with the Rush Hospital, has tackled the task of creating a tool to make easier the diagnosis of CAD through the detection and quantification of these plaques in the CT scans.

1.1 Project motivation

With the facts above mentioned, it is clear that the potential aid of the soft plaque detection is huge. It could help to detect patients with high risk of myocardial infarction in early stages and make an appropriate treatment to avoid a sudden myocardial infarction. In addition, the non-invasive character of this technique allows massive screening in a near future to select patients most likely to benefit from early intervention.

Adding the possibility of soft plaque volume quantification, the outcome is even more attractive. The ability of measuring smaller values than in the common visual inspection makes it very useful in the treatment's progression evaluation. According to Paolo Raggi, from the American College of Cardiology, "Minute regressions in percent stenosis equated to a phenomenal reduction in event rates (referring to myocardial infarctions)." [7]

In this paper, we aim to develop an image segmentation and analysis procedure for identifying soft plaques in coronary arteries from MDCT image data. In the literature there exists a great deal of work on segmentation and visualization of blood vessels in various organs with different modalities (e.g., see [6] for a detailed review). Most of these methods, if not all, focus on how to extract vascular structures from image data.

Unlike calcified plaques, soft plaques exhibit as low intensity and have very little contrast from the arterial wall inside which they reside. Moreover, the vessel may not always exhibit narrowing at soft plaque site; on the contrary, it may even undergo positive remodeling [1]. This consequently poses a significant challenge for soft plaque identification in the presence of imaging noise, as a traditional approach simply based on lumen narrowing analysis no longer works well. Our goal in this work is to demonstrate the feasibility of applying image analysis on both the lumen and arterial wall for detection and quantification of soft plaques from MDCT data.

In this feasibility study, we will focus on a procedure that is computationally efficient, which is critical for practical implementation because modern MDCT scanners can now produce large volumes of data with ever reduced imaging time.

1.2 Plan

The present thesis is organized as follows: In the first part, Background, the framework of the subject is described. The biological characteristics are shown in the Medical section and the existing imaging devices in the Technical section, with especial stress on the MSCT. The next part, Previous Work, introduces the state-of-art in the vessel segmentation and plaque detection and ends with a comparative study of the techniques. The body of the thesis is the section Method, where it is explained the theory and implementation related to the implemented final solution. Finally, in Results and Discussion, a series of tests are run and commented, with a final section detailing future directions of work.

2.1 Medical background

As mentioned in the introduction, heart disease is the leading cause of death in many western countries. Heart disease is a vague term that refer to one of a number of different diseases that affect the heart, being the Coronary Artery Disease (CAD from now on) the most usual.

CAD is the end result of the accumulation of plaques within the walls of the arteries that supply the myocardium (the muscle of the heart) [3]. The accumulation of plaque leads to the narrowing of the arteries, called stenosis, and may progress to the point where not enough blood supply arrives to the heart. In this case, cell starvation of the myocardium produces the myocardial infarction, commonly called heart attack.

The plaques, known as atheroma, are produced by the inflammatory accumulation of macrophage white blood cells (WBC) within the walls of arteries. An atherosclerotic plaque consists of a core of dead foam cells (lipid-engorged macrophages and smooth muscle cells) covered by a fibrous cap. This accumulation may be thrown in the blood stream if the covering tissue, called fibrous cap, is ruptured. The fibrous cap is a region of the intimal layer that has become thickened as a result of medial smooth muscle cells depositing collagen and elastin fibers. A fast development of platelet and clotting over the rupture follows, narrowing the vessel, and a shower of debris may result in an occlusion of downstream vessels.

The thickening artery wall of an atherosclerotic plaque gradually encroaches upon the luminal space and can eventually result in a restriction to blood flow. Unstable plaques, which are susceptible to rupture, are softer, with a thinner fibrous cap. Plaque rupture triggers the formation of a blood clot, which can block the flow of blood through the artery.

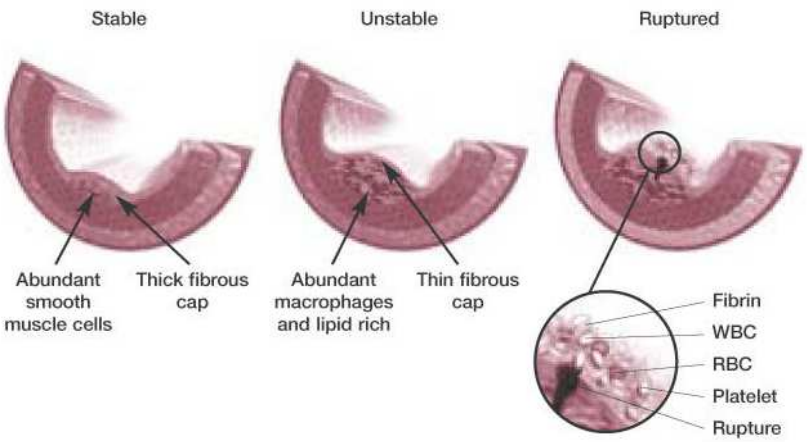

Figure 2: Three different schematic cross-sections stages (Stable, Unstable, and Rupture) of a coronary artery are presented. Source: Ashley, Euan A., Niebauer, Josef et al., Cardiology Explained, Remedica 2004.

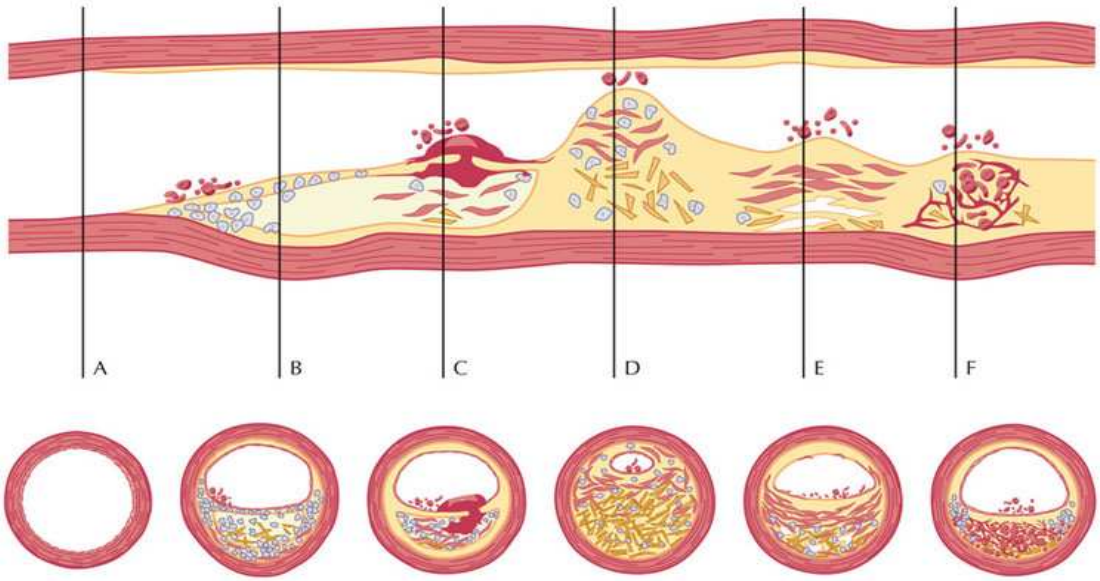

Figure 3: Schematic longitudinal section of an artery showing different stages of atherosclerotic plaque vulnerability. A: Normal, B: Rupture-prone plaque (soft plaque), C: Plaque rupture with fissure, D: Critical stenosis, E: Erosion-prone plaque, F: Intraplaque hemorrhage. Source: Naghavi, Morteza et al., New Developments in the Detection of Vulnerable Plaque Current Atherosclerosis Reports 2001.

Until a little over a decade ago, the danger of plaque progression was considered to be the resulting progressive vessel narrowing, limiting the blood supply to downstream cardiac muscle. The prevailing belief about the culprit plaque was "the smaller, the better". This was proved to be false, or at least not reflective of the whole truth [4].

The large, calcified plaque growing on the inside surface of coronary arteries is not the cause of most heart attacks. Rather, the primary culprit is the soft, relatively small (less than 50% stenosis) "vulnerable" plaque that forms within the vessel walls. Large, calcified plaque is actually relatively stable and, because of its hard calcified covering, less commonly cracks. The more dynamic, less stable soft plaque is much more likely to suddenly rupture.

Medical research since the early to mid-1990s, using medical image, careful clinical follow-up and other methods, have indicated that these lesions are the ones which produce most heart attacks. Unfortunately, vulnerable plaques are not revealed by cardiac stress testing or coronary angiography, the heart tests most commonly performed clinically with the goal of evaluating suspicion to future heart attack.

2.2 Technical background

The detection of vulnerable plaque can be considered a recent problem, hence not extensively explored. Some techniques have been developed in order to help the heart disease diagnosis. A brief review follows, with especial attention to the MSCT.

The techniques may be roughly split into two categories: intravascular or invasive techniques and non-invasive techniques.

2.2.1 Intravascular techniques

All they offer a more accurate exam of the plaque. On the other hand, they require a catheter introduction in the patient's vessel. The main are:

Angioscopy: Angioscopy is the first intravascular imaging device used in clinical practice to further evaluate atherosclerotic plaque beyond angiography. The technique is based on fiber optic transmission of visible light, which provides a small field of view with relatively low resolution for visualization of interior surface of plaque and thrombus.

The advantage of using angioscopy is that its technology is readily available and less expensive than other tests. However, it does have many disadvantages. It only visualizes the surface of the plaque and does not provide enough information regarding plaque characterization, it is

still rather complicated and difficult to use, it has low resolution, and it is highly dependent on the skills of the person performing the test.

Intravascular Ultrasound: Intravascular ultrasound (IVUS) uses miniaturized crystals incorporated at catheter tips, and provides real-time, cross-sectional and longitudinal, high resolution images of the arterial wall with three-dimensional reconstruction capabilities.

There are many advantages to this technique. It is a widely available technology that can be used routinely in clinical practice. It provides detailed information about the content of plaques, in particular, a large lipid core. IVUS can provide information regarding positive and negative remodeling of plaque, and detection of thrombus can be made without much difficulty. However, this test is not perfect. The currently available technology of IVUS does not have enough resolution to visualize the vulnerable plaque cap. Without significant improvement in utilizing ultra-high frequency, IVUS may not identify caps less than 200 mm wide. IVUS is also blind towards the area behind calcified regions, and it does not provide information about the activity of plaque and inflammation.

Intravascular Thermography: This technique is based in the fact that the temperature of a plaque is inversely correlated to its cap thickness. A thermosensor catheter is used to measure the plaque temperature with sensitivity 0.002° centigrade at the presence of continuous blood flow.

The advantages of this test deal with its measurement of temperature. Temperature is one of the most sensitive markers of inflammation; therefore, thermography can provide direct information for detection of inflamed vulnerable plaque. Also, from a technical point of view, measurement of temperature is quite simple and inexpensive. However, because plaque temperature is affected by blood temperature, change in blood flow/temperature may affect temperature readings. Also, thermography may not provide information about presumably no inflamed vulnerable plaque, or lesions with the so-called plaque erosion.

Other intravascular techniques are Optical coherence tomography, Intravascular electrical impedance imaging, Photonic spectroscopy, Elastography and Intravascular and transesophageal magnetic resonance imaging.

2.2.2 Non invasive techniques

These less accurate techniques allow a less traumatic scan and a possibility of massive screening. Some of them are:

Magnetic Resonance Imaging (MRI): During the past 10 years, MRI has become an important tool in the field of cardiovascular disease and atherosclerosis. It relies in the nuclear magnetic resonance and provides angiographic data without radiation exposition. Several pulse sequences have been used to characterize atherosclerotic plaque, such as multispectral MRI using T1, T2, proton density, and three-dimensional time of flight. Some contrast media have been proposed to enhance the diagnostic value.

There are many advantages and a few disadvantages for MRI. It is noninvasive and exposes the patient to no ionizing radiation. It provides information about the lumen of the vessel, as well as its wall (plaque). It allows for the possibility of serial follow-up of patients and plaque, and can provide other information about a patient's cardiovascular, as well as other, systems. The disadvantages of this test include poor coronary access and lack of proper resolution, its long acquisition time, and the fact that it only provides structural information.

Nuclear Imaging: A number of radio labeled materials have been tested for their ability to bind to, and permit, scintigraphic detection of plaque materials. Vulnerable plaques, at least in part, are metabolically very active so they can be detected with a PET system.

However, because of the numerous problems of ionizing radiation and the huge cost issue, radionuclide techniques are unlikely to become the method of choice for detection of vulnerable plaque in the general population.

Electron Beam Computed Tomography: Electron beam computed tomography (EBCT), which quantifies calcification of coronary arteries, has been suggested as a means of diagnosing subclinical coronary artery disease and can reflect the burden of atherosclerosis. However, its use must yet be researched.

Multi-Slice spiral/helical Computed Tomography (MSCT): Radiographic computed tomography (CT) has been subject to rapid technologic advances in the past few years, which

has made it a potential alternative to EBCT. In addition to the development of spiral CT, rotation times in the subsecond range and the development of multi-slice detectors were important advances. The cardiac reconstruction algorithms for imaging the heart with subsecond, multi-slice spiral CT utilizing retrospective electrocardiogram (ECG) information, makes it possible to compete with MRI. With synchronous recording of the ECG, the whole heart can be imaged continuously with thin slices and high spatial resolution in less than 30 seconds. The quality of image appears adequate for precise calcium scoring and CT angiography of the coronary arteries. Although MRI has some other advantages with respect to coronary artery imaging, ultra-fast CT is turning into a real opportunity.

In this work, the value of detection and quantification of the MSCT will be explored. Therefore, a deeper approach to this modality is given below.

2.2.3 Multi Slice Computed Tomography

Computed tomography, also called computed axial tomography, is a medical imaging technique employing tomography where digital geometry processing is used to generate a 3D image of the internals of an object from a large series of 2D X-ray images taken around a single axis of rotation [3].

The first commercially viable CT system was invented by Godfrey Newbold Hounsfield in Hayes, England at Thorn EMI Central Research Laboratories using X-rays. Hounsfield conceived his idea in 1967, and it was publicly announced in 1972. Allan McLeod Cormack of Tufts University independently invented a similar process and they shared a Nobel Prize in medicine in 1979.

X-ray slice data is generated using an X-ray source that rotates around the object; X-ray sensors are positioned on the opposite side of the circle from the X-ray source. Many data scans are progressively taken as the object is gradually passed through the gantry. They are combined together by the mathematical procedure known as tomographic reconstruction.

Newer machines with faster computer systems and newer software strategies can process not only individual cross sections but continuously changing cross sections as the gantry, with the object to be imaged, is slowly and smoothly slid through the X-ray circle. These are called

helical or *spiral CT* machines. Their computer systems integrate the data of the moving individual slices to generate 3D volumetric information, in turn viewable from multiple different perspectives on attached CT workstation monitors. A heart volume is shown in the figure 4.

To show the results, pixels in an image obtained by CT scanning are displayed in terms of relative radiodensity. The pixel itself is displayed according to the mean attenuation of the tissue(s) that it corresponds to on a scale from -1024 to +3071 on the Hounsfield scale (the unity is the HU).

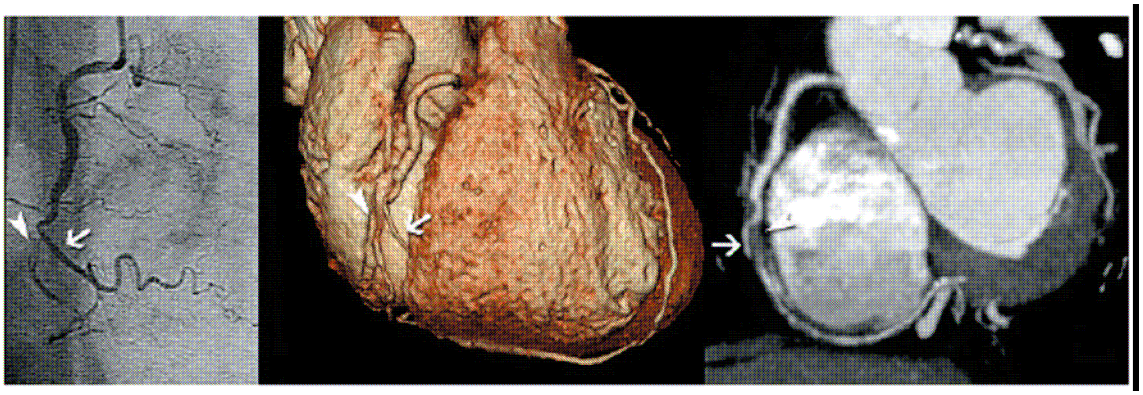

Figure 4: Conventional angiography image (left panel). Corresponding CT images using different image post-processing techniques: volume rendered (middle panel) and maximum intensity projection (right panel). Source: Mollet et al., Non-invasive multislice CT coronary imaging, BMJ Publishing Group & British and Cardiac Society, 2005.

Multislice CT represents the latest breakthrough in CT Technology. Fundamentally, MSCT scanner is equipped with a multiple detector array that concurrently collects data at different slice locations, a defining feature that brings in numerous advantageous spin-offs like rapid scanning, large patient coverage volume, high z-axis resolution, and generation of true isotropic datasets which in combination facilitates 3D imaging. MSCT provides a huge gain in performance that can be used to reduce scan times, reduce scan collimation or to increase scan length substantially [5].

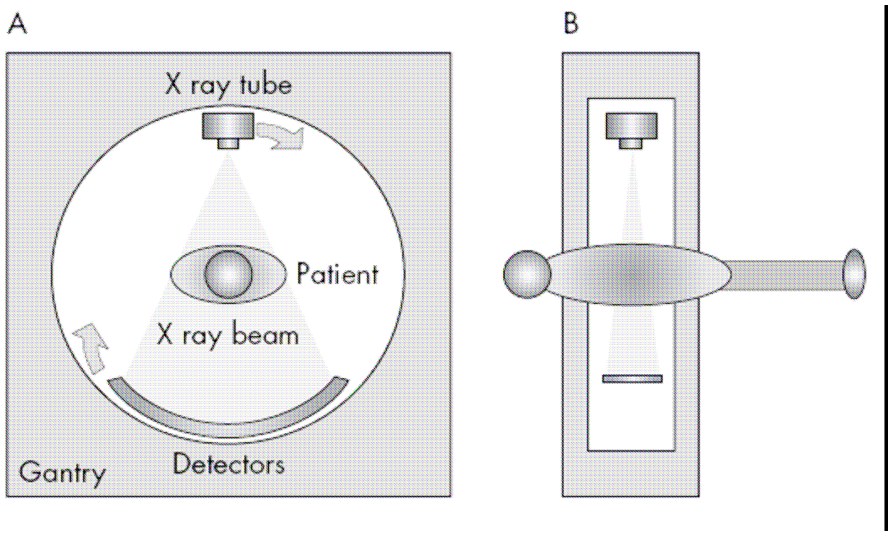

Figure 5: Frontal (A) and side (B) view of a computed tomography (CT) scanner. Source: Mollet et al., Non-invasive multislice CT coronary imaging, BMJ Publishing Group & British and Cardiac Society, 2005.

In the work of Schroeder et al. [6], the accuracy of non invasive MSCT and invasive IVUS in the soft plaque detection is compared. Experiences were performed in 15 patients with a total burden of 34 plaques. As a result, they stated that MSCT can differentiate coronary lesion configuration, with an especial mention to the soft plaque evaluation, which could make the MSCT an important diagnostic tool for risk stratification.

Following the article of Budoff [12] states, the identification of a non-calcified plaque may very well be a plaque at an earlier stage of atherosclerosis, more amenable to anti-atherosclerotic therapies. Identifying a person with a large area of lipid-laden plaque and then initiating lipid-lowering therapy to treat the asymptomatic CAD has logical appeal. However, one question is whether CT angiography can properly differentiate different types of non-calcific atherosclerotic plaque. Fibrous plaque generally is considered more stable (less vulnerable), whereas soft plaques with a large lipid core are far more vulnerable to rupture. Several CT studies have demonstrated that the lipid-rich plaque has a lower, but overlapping attenuation pattern to fibrous-rich plaque. Although there is no issue about detecting non-calcium plaque from the blood pool or calcium, there is substantial overlap between lipid-laden and fibrous plaque, not always permitting consistent differentiation [13]. Considering this, further studies are needed to demonstrate inter-reader and inter-scan reproducibility of the measure, autopsy studies are needed to validate quantification and identification of plaque burden, and validation of CT modalities ability is needed to separate coronary plaque composition into lipid- or fibrous-rich plaques.

For now, due to the recent innovation in both medical and technical background, the number of research studies about the soft plaque detection with MSCT scanners is still limited. The soft plaque volume quantification is virtually inexistent. Nevertheless, many have started to be interested.

The big companies in the medical imaging field have begun to study, or even commercialize, some products for the soft plaque detection. For instance, Siemens with the HeartView CT Cardiac Imaging, which offers coronary plaque visualization, or Toshiba with its SurePlaque –still in-progress– which provides color-coding of vessel walls, non-calcified and calcified plaques.

Other projects related to soft plaque detection are being developed in other institutions, as "Detection of vulnerable plaque in the carotid artery with multislice CT" in the Erasmus University of Rotterdam or the project directed by Hans et al. [8] in Harvard Medical School.

3.1 Vessel's intensity

The segmentation consists on separate an object with special features from an image. For the vessel's segmentation, the used feature is the vessel's intensity. This is evaluated using subjective evaluation criterion. In fact, lot of segmentation's techniques use two a priori knowledge:

- the inner of the vessel is brighter than the wall of the vessel.
- the background is darker than the vessel.

Even though most of the algorithms use the intensity, few articles discussed about the fact that vessel's intensity has a gaussian distribution ([14], [15] and [16]).

The second article defines the vessel's intensity as a piecewise of Gaussian, but still consider the vessel as a one part. Moreover the study is for retinal vessels. The last article defines the

vessel's intensity as the same as a blood-filled-region (vessel but also ventricle). The paper separates the thorax image only in three parts: myocardium, blood and lung. We will see in section 3.2 another way to separate the different parts of a vessel (inner, wall and stenoses).

3.2 Vessel segmentation

An extensive collection of papers has been published on the subject of segmentation and analysis of vessels, foundation of the soft plaque detection. An excellent overview is given by Kirbas and Quek [9]. In this survey, they divided the existing vessel segmentation algorithms and techniques into six main categories: pattern recognition techniques, model-based approaches, tracking-based approaches, artificial intelligence-based approaches, neural network-based approaches, and tube-like object detection approaches. These categories embrace the main trends in vessel segmentation, although many techniques use a mix of them.

We can separate all this methods in two main classes of approach: one based on "local measure" (region growing, differential geometry-based approaches, model-based approaches...) and the other based on "global measure" (Parametric deformable models, level-set methods, front propagation methods...) . In general, the local measure is faster than the global one, because it uses a minimized region of interest.

Growing and thresholding methods, in their most general form, are not sufficient to extract only the whole coronary arteries, because of the properties of these images. Finding appropriate methods is known to be a challenging problem because of the data imperfections such as noise, heterogeneous intensity and contrasts of similar tissues.

Following this classification and comparing with other more recent papers (Kirbas review was published in 2004), we searched for the current trends and the most reliable techniques, in function of the citations in other papers and the tests performed. The first aim was to get a method that could be used in the soft plaque detection in MSCT images. The second aim of this project is to combine an accurate method with a fast one. No method appeared as the perfect one but, according to the mentioned criteria, it was observed the prevalence of some techniques: front propagation method, region growing and differential geometry-based approaches, detailed below.

3.2.1 Region Growing

Region growing technique segments image pixels that belong to an object into regions. Segmentation is performed based on some predefined threshold. The threshold is in general a percentage of the intensity of the seed point. This technique has been used in some papers, such as Extraction of Blood Vessel in CT angiography image aided by fuzzy logic ([10]) or System for Analyzing High-Resolution Three-Dimensional Coronary Angiograms ([11]).

This technique is not really robust against noise (threshold is an approximation), so there are lot of pre-treatments such 3D smooth image filter, threshold operations to separate brighter and darker region. Another problem with this technique is the difficult way to extract some features, in order to study the vessel characteristics and to detect soft plaques.

3.2.2 Differential geometry-based approaches

Approaches based on differential measures typically use partial derivatives of the image data up to second order. In the segmentation of vessel, the Hessian matrix is used, used, which requires second-order partial derivatives of an image. In general, the used kernel is Gaussian, which permits a good detection of edges. In this approach, eigenvalues and eigenvectors are exploited, and a vesselness measure can be calculated with the eigenvalues. The main problem of this technique is that is very sensitive to the noise (the region of interest is very small, and biased value have more consequences). The robustness can be improved with by using a multi-scale approach.

3.3 Soft Plaques Detection

For the detection of the soft plaque, the main idea is to extract the centerline of the vessel, then to calculate its diameter or its radius, and finally to detect where the vessel narrow down. There are many problems for this detection. First of all, the accuracy of the centerline is very important. The diameter depends directly of the centerline. To find it, the main algorithms use iterative algorithms, which can take a lot of time. The second problem to find a precise centerline is to have a good segmentation. But the threshold of the segmentation is not really precise.

The second main problem is the use of the diameter. The vessel lumen may not be a regular cylinder. In fact, the soft plaques are usually eccentric and asymmetric (see the figure 6, part A) . The use of the diameter is an approximation. Consequently there are other features which are extracted like cross-section areas ([17] and [18]). This method is more robust than the diameter. But it depends hardly on the cross section segmentation. If the plane is not perpendicular, the cross-section area will increase really fast (see the figure 6, part B).

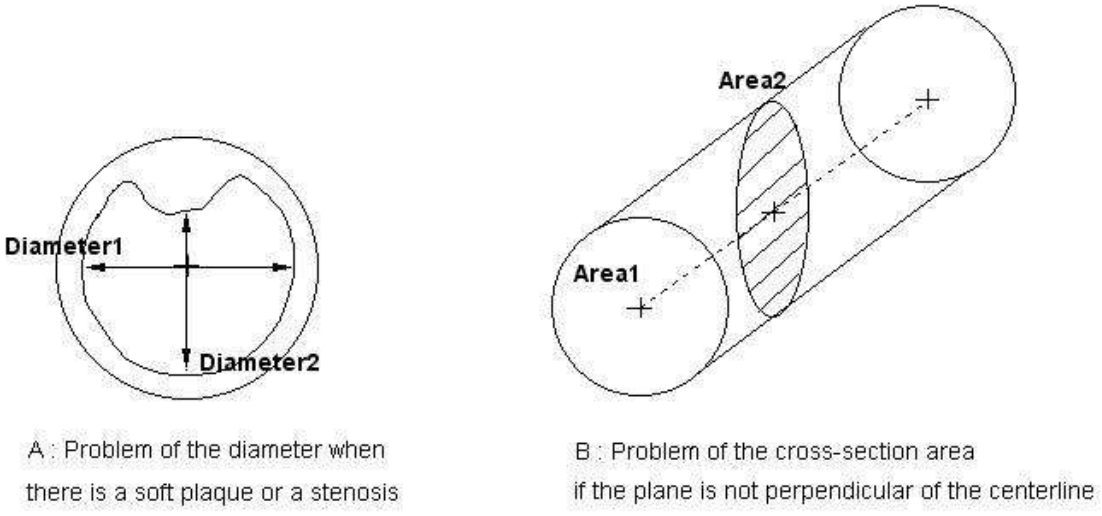

Figure 6: Problems of using diameter and cross-section area for detection of soft plaques

We will introduce a new feature in our approach: local volume of the vessel (see the part 3.3).

For the segmentation of the soft plaques, a first approach uses a convex algorithm is described in the paper Detection of vulnerable plaque in the carotid artery with MSCT by Hans et al. [8]. They have good results but the region of interest is small, consequently they can segment only small soft plaques.

Since soft plaques are known to lie within the arterial wall [2], our procedure begins with segmentation of the major coronary arteries, which includes separate segmentation of the lumen and arterial wall. We then identify the presence of soft plaques by examining the geometric and image features of the lumen and its surrounding wall surfaces. Our proposed semi-automatic procedure consists of the following five steps that are explained below:

1) Approximate detection of the arterial lumen's centerline using a multi-scale tracking algorithm
2) Segmentation of the vessel's lumen by means of an EM segmentation
3) Correction of the initial centreline by means of the lumen segmentation
4) Segmentation of the lumen and the wall separately with an EM segmentation method
5) Identification of soft plaques by comparing the cross-sectional areas of the lumen and wall.

The method is semi-automatic, as the user has to manually select the seed point from real MSCT scan slices. The rest of the algorithm is automatic.

3.1 First extraction of the vessel centerline

With contrast enhancement the lumen voxels of the coronary arteries appear brighter than their immediate surroundings, and as a consequence the blood vessels can be modeled by a tubular structure in MDCT images. As mentioned earlier, there are many methods developed in the literature for vessel tracking based on this property (e.g., [22]). Out of consideration of computation complexity, we adopt a centerline tracking approach that is similar in spirit to [16] and [17], where vessel tracking is guided by a multi-scale filter based on local eigenvalue analysis of the Hessian matrix of the image.

The main advantage of this method is that it is very fast. Indeed, the algorithm calculates the vessel locally and avoids the problem of working with a large amount of data, that would make the overall computation slow. Moreover, this algorithm gives us the normal vector of the consecutives orthogonal planes of the lumen's centerline. They will be used to calculate the local volume. The main drawback of the multi-scale tracking algorithm is its accuracy, as it

gives an approximate centerline of the vessel. As having the true centerline of the artery is essential to obtain a precise EM segmentation of the lumen and wall in posterior steps, further corrections of this initial tracking extraction are required (See 3.3).

This first step requires the user to select the seed point where the tracking algorithm can start from, making the overall method semi-automatic. The algorithm implements the extraction of the centerline of the vessel starting from the seed point selected by the user. It can be divided in two parts:

- the estimation of the position of the centerline's point.
- the local direction estimation.

As a first approach, we just look for the tracking of one single branch of the vessel. In future work, extracting the whole vessel's tree will be a priority like in the paper of Yang [14].

3.1.1 Estimation of the centerline's point

First of all, we take a seed point inside the vessel we will segment. Then we take a window region of interest around this seed point, and find the center of gravity of this window. Indeed, we suppose that the inner vessel is brighter than the background (this point is developed in section 3.2), and consequently that the centerline's point corresponds to the center of gravity of the window.

Moreover, we assume that the vessel is a cylinder, so we take a spherical window. But the results is similar with a cubical window, but the dynamic is different (we find centerline's points but not the same points that we get with spherical window).

We applied the first geometric central moments to compute this local centroid. The coordinates of the local centroid $\left(\vec{x},\vec{y},\vec{z}\right)$ inside a spherical window is given by:

$$\left(\vec{x},\vec{y},\vec{z}\right)=\left(\frac{M_{100}}{M_{000}},\frac{M_{010}}{M_{000}},\frac{M_{001}}{M_{000}}\right)$$

where M_{rpq} is the r order moment in the $\vec{x}$ direction, p order moment in the $\vec{y}$ direction, and q order moment in the $\vec{z}$ direction. We can read the paper of Hew [20] to learn more about the gravity center. The window center and the local centroid can be different, so we make an iterative process (see the figure 7). We replace the window center by the last local centroid. Due to the hypothesis that the centerline is brighter than the background, this iteration matches the local centroid with the center line of the vessel.

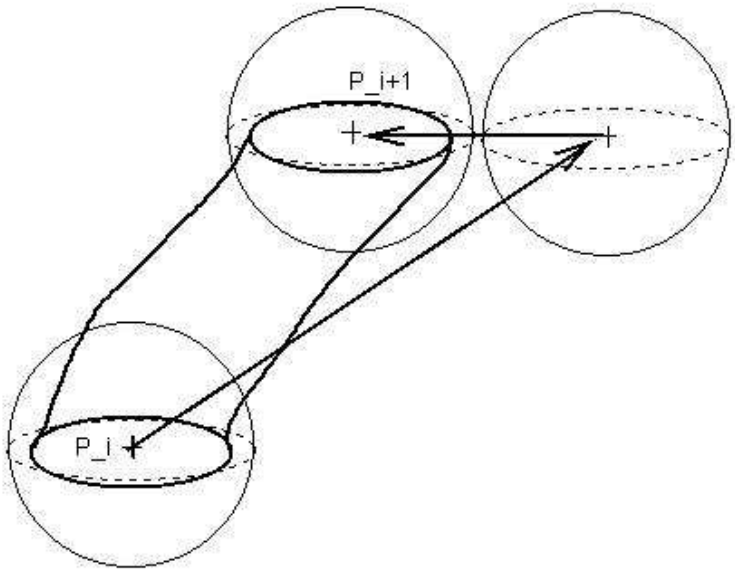

Figure 7: One step of the algorithm between two points of the center line (in bold the vessel, we use a spherical window)

You can have a problem of robustness if the size of the window is too small or too large. If it is too small, the iteration is very long and is very sensitive to the noise. If it is too large, a heart cavity can be located inside your window, which is brighter than the vessel. Moreover local centroid can have a problem to stabilize itself (it can go fast and let a big gap). Consequently we choose a window radius close to the vessel radius, but higher than it to avoid some noise.

3.1.2 Local vessel direction estimation

A multi-scale filter based on eigenvalue analysis of the Hessian matrix was locally applied to the estimated point of the centerline. It permits to estimate the orientation of the vessel. We define the Hessian matrix for a voxel **X** at scale σ such as:

$$H_\sigma(X) = \begin{pmatrix} I_{xx}(X)\, I_{xy}(X)\, I_{xz}(X) \\ I_{xy}(X)\, I_{yy}(X)\, I_{yz}(X) \\ I_{xz}(X)\, I_{yz}(X)\, I_{zz}(X) \end{pmatrix}$$

where I_ is the regularized derivatives of the image I(**X**), which are obtained by convolving the image using the Gaussian kernel G(**X**, σ) at scale σ:

$$I_{\alpha\beta}(X) = \sigma \frac{\partial^2 G(X,\sigma)}{\partial\alpha\partial\beta} * I(X)$$

with Gaussian kernel:

$$G(X,\sigma) = \frac{1}{\sqrt{(2\pi\sigma^2)^3}}\, e^{\frac{|X|^2}{2\sigma^2}}$$

The second derivative of a Gaussian kernel at scale σ permits to detect the contrast between the regions inside (vessel) and outside (background) in the direction of the derivative.

Now, let λ_1, λ_2, λ_3 and $\vec{v_1}$, $\vec{v_2}$ and $\vec{v_3}$ be the eigenvalues and the unit eigenvectors of $H_\sigma(X)$. he eigenvector $\vec{v_1}$ corresponds to the smallest eigenvalue λ_1 and it follows the direction of the vessel (see the figure 8). The properties of the eigenvalues of $H_\sigma(X)$ give important information about the vessel structure at the found centerline point $\mathbf{p}_i$, such as tubular vs. plate-like structure (at vessel bifurcation); moreover, the eigenvector associated with the smallest eigenvalue (in magnitude) $\vec{v_1}$ corresponds to the principal direction of the vessel, and

the other two eigenvectors correspond to the cross-section of the vessel, so $\vec{v_2}$ and $\vec{v_3}$ form a base of the orthogonal plane to $\vec{v_1}$.

Frangi et al. [21] introduced two geometric ratios R_A, R_B in their vessel likeliness function $V(X,\sigma)$ that follows :

$$V(X,\sigma)=\begin{cases}0 & \text{if } \lambda_2 \geq 0 \text{ and } \lambda_3 \geq 0 \\ (1-e^{\frac{-R_\sigma^2}{2\alpha^2}})(e^{\frac{-R_\beta^2}{2\beta^2}})(1-e^{\frac{-S^2}{2c^2}}) & \textit{else}\end{cases}$$

The ratios R_a, R_b and S are define as:

$$R_a=\frac{|\lambda_2|}{|\lambda_3|} \qquad R_b=\frac{\lambda_1}{\lambda_2\lambda_3} \qquad S=\sqrt{\lambda_1+\lambda_2+\lambda_3}$$

The parameters α, β and c control the sensitivity of the filter. It is fixed arbitrarily. The parameters R_a, R_b and S describe the geometry of the vessel, but we don't use this information in our paper. The interested reader can refer to the paper [14], [21], [22] and [23].

The response of this filter was computed at different scales σ. The response of the filter is maximum for the scale σ which approximates the vessel. So we have:

$$\sigma_{used}=\max_{\sigma_{min}<\sigma<\sigma_{max}}(V(X,\sigma))$$

The direction of the vessel corresponds to the eigenvector $\vec{v_1}$ at the scale σ_{used}.

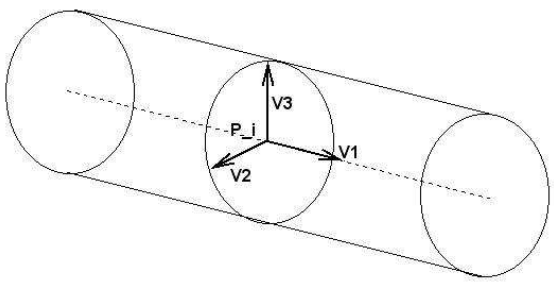

Figure 8: Eigenvectors of H_σ at the point Pi

It is expected that the estimated principal direction above will be sensitive to the imaging noise, because the Hessian matrix $H_\sigma(X)$ involves the second derivatives of the image. To reduce the impact of the noise, we apply a post-filtering step on the search direction vector. Specifically, let $\mathbf{v}_i'$ denote the computed principal direction at $\mathbf{p}_i$ from eigenvalue analysis as above. Then the search direction $\mathbf{v}_i$ is obtained by using the following autoregressive filter:

$$\mathbf{v}_i = \alpha \mathbf{v}_i' + (1-\alpha)\mathbf{v}_{i-1}$$

where $\mathbf{v}_{i-1}$ is the search direction at previous centerline point $I(\mathbf{p}_{i+1})$, $0 < \alpha < 1$ is a constant used to control the update speed. In our experiments, $\alpha = 0.5$ was used.

To avoid backward tracking, the eigenvector $\mathbf{v}_i'$ is chosen to be in the general direction of $\mathbf{v}_{i-1}$, i.e., $\langle \mathbf{v}_i', \mathbf{v}_{i-1} \rangle > 0$; otherwise, its opposite direction is used. In our experiments, for centerline extraction a cubic window with 10 voxels in each dimension was used for computing the center of gravity. Now we have to choose an incremental displacement along the vessel's centerline. As the radius of the window, we have to choose wisely this parameter. If it is too small, the time of the algorithm can be very long, and we can be blocked. If the step is too long, we can go to the nearest cavity (see the figure 9) and the posterior cross-sectional area measurement could be less accurate in when the cross-sectional planes are not exactly orthogonal to the real centerline of the vessel.

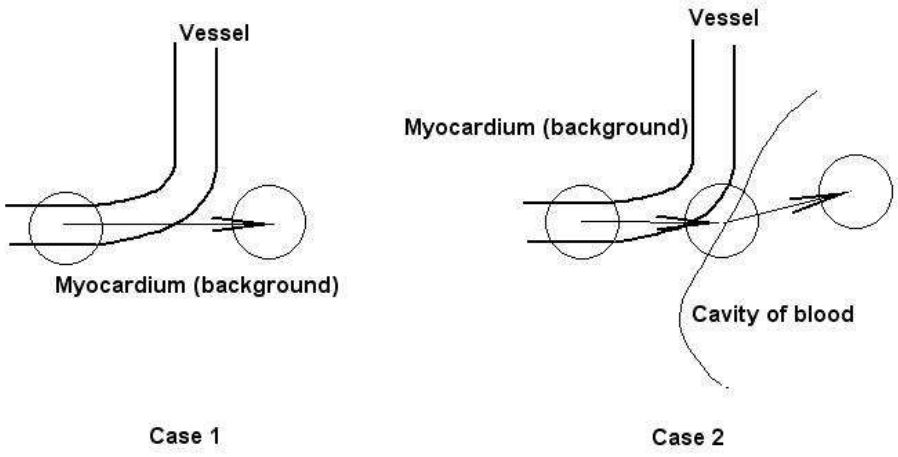

Figure 9: Two divergent cases if the length of the displacement is too long

After considering the time cost of having a short step size and evaluation the posterior volume measurement relying on the cross-sectional area of every tracking step, the step size used was 2 voxels between two consecutive centerline points.

We iterate the estimation of the position of the centerline's point and the local vessel direction estimation until some stop criterions. By estimating the radius, area and perimeter of every tacking step, we implement three stop criterions:

- Entering big cavities next to the vessel when the radius R>15 voxels
- Entering a tracking loop when the next centerline point $\mathbf{p}_{i+1}$ has been already tracked
- Entering to a myocardium (background) area when the next point intensity is too low $I(\mathbf{p}_{i+1})$ <900 and our of the vessel's intensity range
- Next tracking point is out of the scan image bounds

After finding stopping criteria, the algorithm goes back to the initial seed point and starts tracking to the reverse tracking way, until we meet other stopping criteria. So, the tracking procedure starts with a seed point $\mathbf{p}_0$ selected on the lumen of a coronary artery, and searches for a set of centerline points along the path of the lumen in the following successive fashion: at point $\mathbf{p}_i$, $i = 0,1,\cdots$

a. Refine the point $\mathbf{p}_i$ so that it lies on the centerline of the lumen.
b. Perform multi-scale Hessian filter analysis to obtain the local main local direction $\mathbf{v}_i$ of the lumen at $\mathbf{p}_i$.
c. Search the next tracking point with direction $\mathbf{v}_i$, i.e., $\mathbf{p}_{i+1} = \mathbf{p}_i + d_i\mathbf{v}_i$, where d_i is the step size.
d. Repeat the above steps until the stop criterion is met.
e. Go back to seed starting point $\mathbf{p}_i$ picking the reverse local principal direction $\mathbf{v}_i$ of the lumen and repeat the above steps

We present an operating diagram of this two steps and of the stop criterions in figure 10:

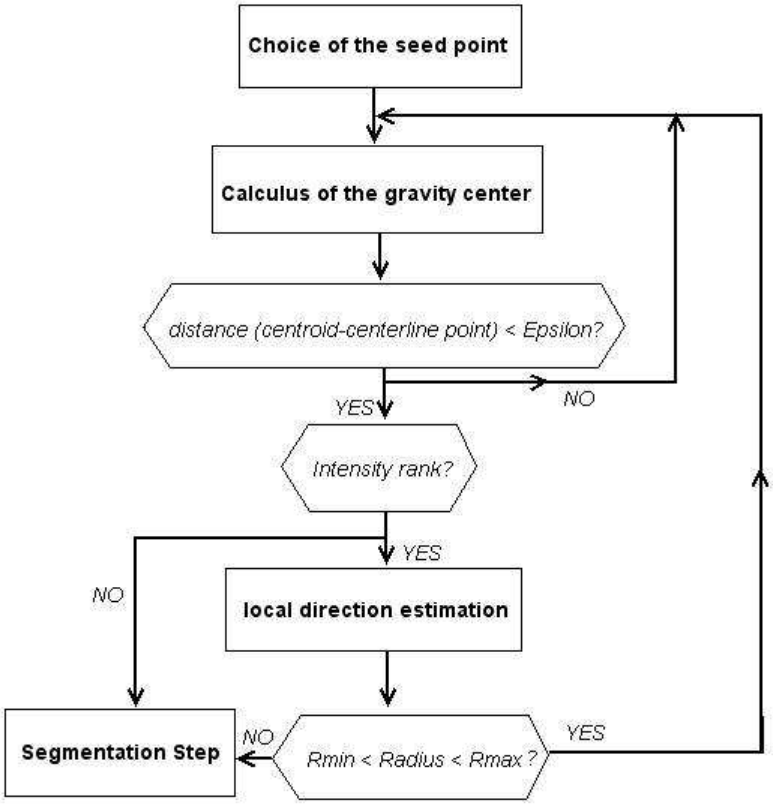

Figure 10: Operating diagram for the extraction of the centerline

It is important to notice again that this tracking algorithm doesn't detect nor track bifurcations on the seed's point vessel, so it ignores the ramifications from the artery. This approach is more simplistic. Albeit the simplification was deliberate. This project is not intended to create a vessel tree but to validate the centerline extraction and improve the vessel segmentation and soft plaque detection. Further extension of the artery tree tracking will be desirable.

3.2 Pre-segmentation operations

The local differences in contrast agent distribution and other undesired features lead to a noisy data. Therefore, the first task of the preprocessing should be improving the image quality. Several filtering options were considered but, after analyzing the filtering steps already done by the post-processing of the Phillips MSCT 64-slice scan such as z-axis multi-slice filtering, at last, the 2D median filtering gave the best results. The median of a group, containing an odd number of elements, is defined as the middle element, when the elements of the group are

sorted. A median filter finds the median of a number of elements at its input. In the standard median filtering applications, a window of size $[w, w]$, where w is odd, is moved along the sampled values of the image. The median filter considers each voxel and looks for the values of its 2D neighbors. Then, it calculates its median value, i.e. the number dividing the higher half of the ordered sample, and replaces the considered output voxel located at the same position as the central element of the window with it [24]. The median computed at this operation is called the running or the moving median. Since the size of the window is constant, the number of incoming elements is equal to the number of outgoing elements. [25]

Our filter takes the neighbors in the cube of size 4x4. The result is a new image that eliminates the impulse noise and conserves accurately the edges.

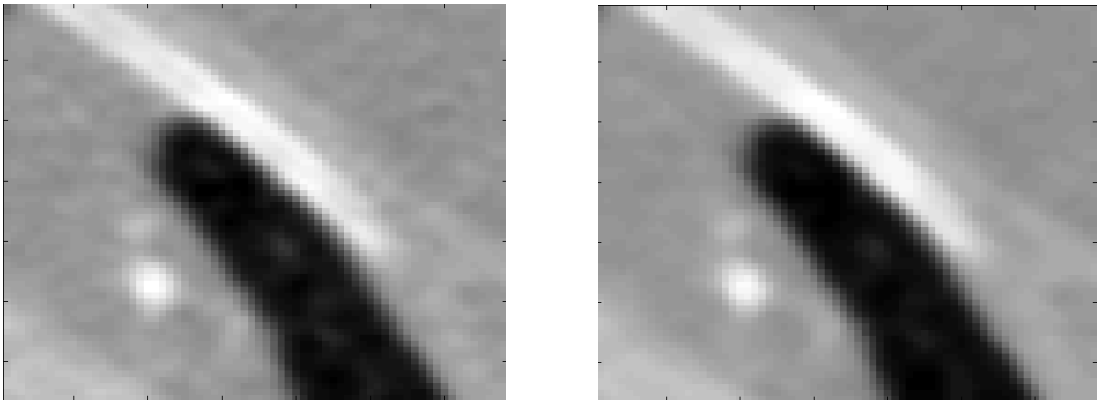

Figure 11: Original image scan (left) and median-filtered image scan (right).

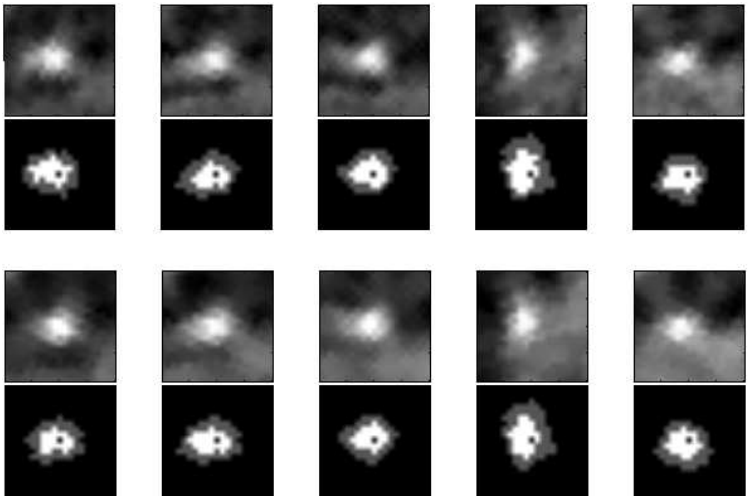

Figure 12: Cross-sectional original (top) and median-filtered image (bottom) segmentation view results.

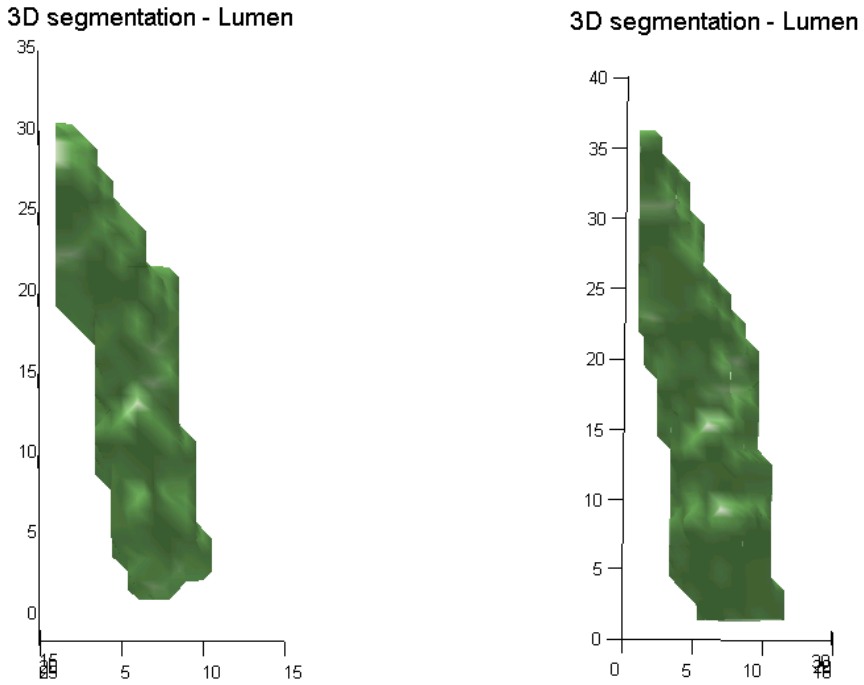

Figure 13: 3D lumen segmentation view results without (left) and with median-filtered image (right).

Before entering to the segmentation step of the algorithm, we resize the constructed 3D image volume data to the region of interest as computational efficiency increases, defining the new bounds of the dataset with a rectangular prism containing the previously tracked vessel.

3.3 EM segmentation

After the first centerline extraction, we have obtained a sampled approach to the real centerline of the vessel, orthogonal planes to the direction of the centerline at each tracking point and the approximate radius of the lumen. With this basis, we perform an Estimation Maximization (EM from now on) for Gaussian Mixture estimation process to eventually segment separately the lumen and the wall of the coronary artery selected with the seed point.

The EM for Gaussian Mixture Model (GMM) is a iterative statistical process in which a histogram of gray intensity values is modeled as mixture of Gaussians by means of an data input of voxels. By using this GMM, we assume that the lumen and wall intensity distribution is Gaussian. Prior to the EM for GMM description, let's analyze this assumption by stydying the vessel intensity distribution.

3.3.1 Vessel intensity distribution

Some papers present that the vessel has a Gaussian distribution for its intensity rank ([14], [15] and [16]).. The second paper [15] describe the vessel in a piecewise Gaussian distribution. But all this papers don't make a difference between the wall and the inner of the vessel. For the detection and the segmentation of the soft plaques, this difference is pivotal. In fact, the soft plaques have the same intensity as the wall.

In our paper, we study the wall vessel intensity (lumen and wall) and the myocardium (background), which are the surrounding coronary components surrounding the vessel centerline. These heart components voxels are critical as they are the ones that our segmentation algorithm will have to classify after having tracked the artery centerline. The main goal of this point is to check if the vessel has an approximate Gaussian intensity distribution as the previous mentioned papers present. Firstly, we study the case of the inner vessel (lumen) and the wall of the vessel.

First of all, we explain how we have the intensity rank for the different cases. To have experimental intensity rank of the vessel, we segment the vessel with the tracking multi-scale algorithm to get the centerline, and we process a region growing algorithm with a threshold of 90% and 110% of the centerline's intensity.

This threshold is rough, but sufficient to have enough voxels to make some experiments in order to show that the intensity for each of this three heart components has a Gaussian kind of distribution. When we try to get intensity distributions on a huge image, the vessel intensity range is included in the big heart cavities intensity range. So the curve obtains for the wall and the myocardium is better than the curve for the wall and the inner vessel (there are more samples in the first one). With this experimentation, we acquire a good knowledge of the background (myocardium).

We fit the wall vessel intensity and the myocardium with a sum of two Gaussians (figure 14). Each Gaussian corresponds to one component. The segmentation of each part using this intensity range difference allows us to have a good separation of coronary components. The formula is the following:

$$GMM(x) = A_1 e^{\left(-\frac{|x-m_1|^2}{2\sigma_1^2}\right)} + A_2 e^{\left(-\frac{|x-m_2|^2}{2\sigma_2^2}\right)}$$

where A_1 and A_2 are the amplitudes, m_1 and m_2 the means, and σ_1 and σ_2 the variance.

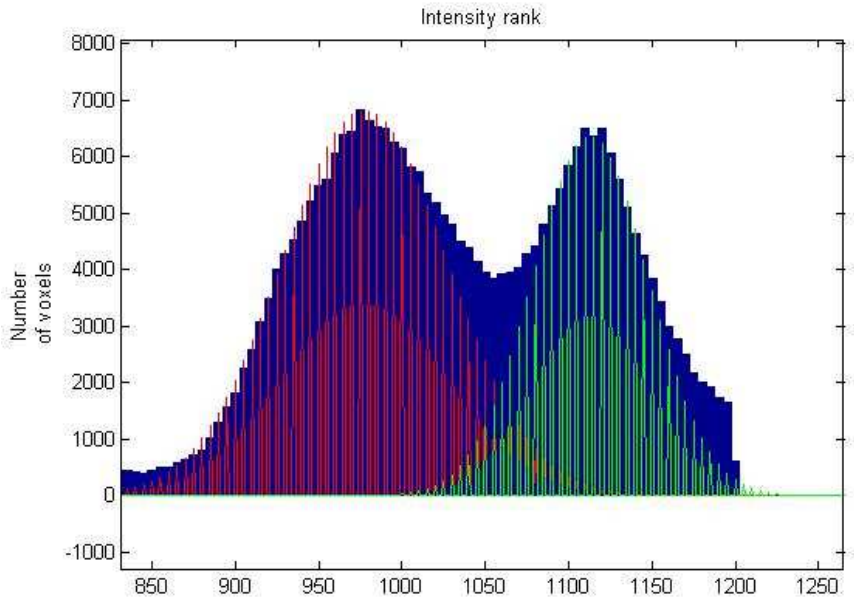

Figure 14: In blue the experimental intensity histogram for voxels of both the myocardium and the wall where two Gaussians are distinguishable, in red the Gaussian theoretical model for the myocardium part, in green the Gaussian theoretical model for the wall.

As we can see in the figure 15, both myocardium and wall experimental intensity distributions have an approximate Gaussian shape. The myocardium intensity range has a lower mean than the wall's, as the wall voxels are brighter. Now we are going to study the case of the wall and the inner vessel. We have less samples than for the last case, so the histogram is noisier.

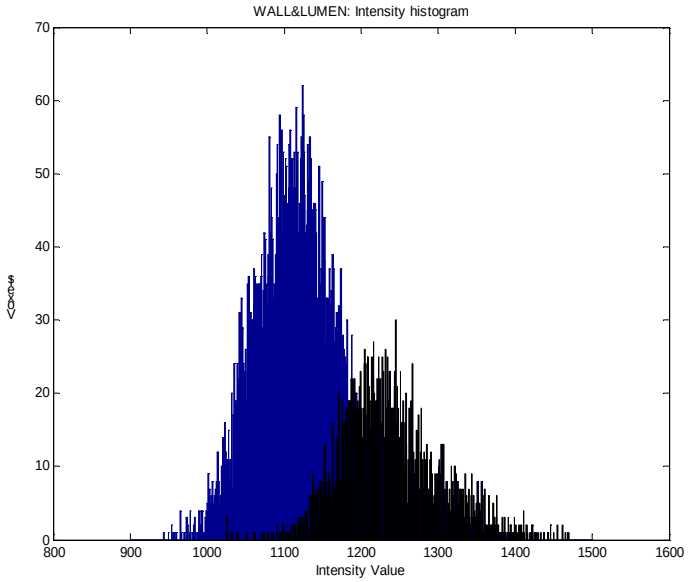

Figure 15: The experimental intensity histogram for the wall (in blue) and the inner (in black) of the vessel.

In this last case of the vessel's wall and lumen intensity distribution, we can distinguish again two approximate Gaussian functions in the histogram. The wall intensity range has a lower mean than the lumen's, as the lumen voxels are brighter. Finally, we plot the experimental histogram of the surrounding vessel's centerline voxels to show the 3 Gaussian components corresponding to the background, the wall and lumen.

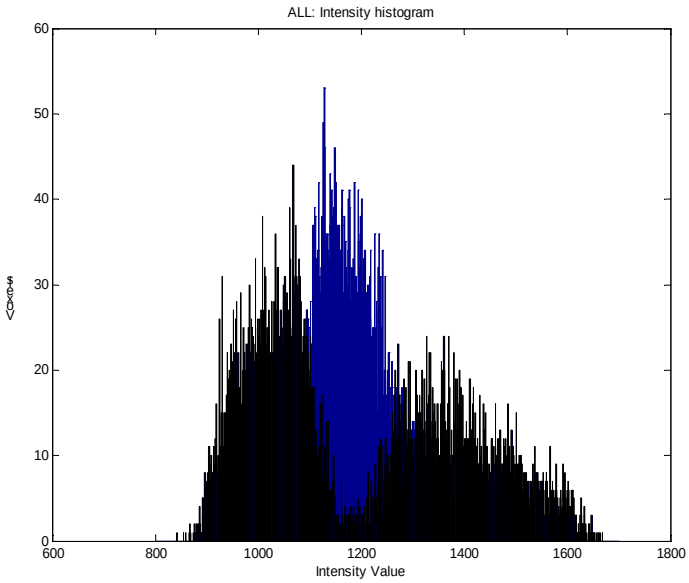

Figure 16: Experimental intensity histogram of the wall (blue), inner and background (black) of the vessel.

In other papers [14], a differentiation of three intensity coronary components is done (blood, lung and myocardium), but they didn't separate the wall and the inner vessel case. After this experimental study with real MSCT scan, we proved the piecewise of Gaussian used in [15], and we can separate the surrounding voxels of the vessel in three coronary components (inner, wall and myocardium by modeling them with three Gaussian intensity distribution functions of weight A, mean m_1 and deviation σ, as follows:

$$GMM(x) = A_1 e^{\left(-\frac{|x-m_1|^2}{2\sigma_1^2}\right)} + A_2 e^{\left(-\frac{|x-m_2|^2}{2\sigma_2^2}\right)} + A_3 e^{\left(-\frac{|x-m_3|^2}{2\sigma_3^2}\right)}$$

where the myocardium is the Gaussian with lower intensity mean and the lumen is the Gaussian with higher intensity mean. Assuming now that we can model the intensity distribution of this three coronary components, we can apply the EM segmentation for Gaussian mixture model to classify every surrounding voxel of the vessel centerline.

3.3.2 Estimation Maximization for Gaussian Mixture Model

In the general case, the Expectation Maximization (EM) Algorithm is a method of finding the maximum-likelihood estimate of the parameters of an underlying distribution from a given data set when the data is incomplete or has missing values. The EM algorithm is an optimization algorithm that attempts to find a set of model parameters that corresponds to a maximum in the likelihood function. However the EM algorithm assumes that some variables are not observable, so the likelihood function cannot be exactly calculated and it is estimated with its expectation. Actually, it is the likelihood expectation that is maximized rather than the true likelihood. The EM is an iterative algorithm where each iteration consists of an Estimation step, were the expected likelihood function is calculated, and the Maximization step where it is maximized.

Once selected the input voxels for the EM algorithm, for the Probability Density Function of mixture Gaussian function, the likelihood function is defined as follows:

$$\Lambda(\mathbf{x};\ \Theta) = \prod_{n=1}^{N} \sum_{i=1}^{d} P_i \cdot p\left(x_n;\ \mu_i,\ \sigma_i^2\right)$$

The logarithm of the likelihood function $\Lambda(\mathbf{X};\ \Theta)$ is given by

$$\lambda(\mathbf{X};\ \Theta) = \sum_{n=1}^{N} \log \sum_{i=1}^{d} P_i \cdot p\left(x_n;\ \mu_i,\ \sigma_i^2\right)$$

To find expressions that are valid at local maxima of λ (or equivalently Λ), we compute the derivatives of λ with respect to P_i, μ_i, and σ_i. Setting the derivatives equal to zero, we obtain three groups of equations for the mixing probabilities, means, and standard deviations (Tomasi [28]):

$$P_i = \frac{1}{N} \sum_{n=1}^{N} P(i \mid n) \qquad \mu_i = \frac{\sum_{n=1}^{N} P(i \mid n) \cdot x_n}{\sum_{n=1}^{N} P(i \mid n)} \qquad \sigma_i = \sqrt{\frac{1}{d} \cdot \frac{\sum_{n=1}^{N} P(i \mid n) \cdot \left\| x_n - \mu_i \right\|^2}{\sum_{n=1}^{N} P(i \mid n)}}$$

At this point, we assume that approximate (initial) estimates $P_i^{(k)}$, $\mu_i^{(k)}$, and $\sigma_i^{(k)}$ are available for the parameters of the likelihood function $\Lambda(\mathbf{X};\ \Theta)$ or its logarithm $\lambda(\mathbf{X};\ \Theta)$. Then, better estimates $P_i^{(k+1)}$, $\mu_i^{(k+1)}$, and $\sigma_i^{(k+1)}$ can be computed by first using the old estimates to construct a lower bound $b_k(\Theta)$ for the likelihood function, and then maximizing the bound with respect to P_i, μ_i, and σ_i.

Expectation maximization (EM) starts with initial values $P_i^{(0)}$, $\mu_i^{(0)}$, $\sigma_i^{(0)}$ for the parameters, and iteratively performs these two steps until convergence. Construction of the bound $b_k(\Theta)$ is called the "E step," since the bound is the expectation of a logarithm, derived from use of Jensen's inequality. The maximization of $b_k(\Theta)$ that yields the new estimates $P_i^{(k+1)}$, $\mu_i^{(k+1)}$ and $\sigma_i^{(k+1)}$ is called the "M step."

Given the old parameter estimates $P_i^{(k)}$, $\mu_i^{(k)}$ and $\sigma_i^{(k)}$, we can compute estimates $P^k(i \mid n)$ for the membership probabilities

$$P^{(k)}(i \mid n) = \frac{P_i^{(k)} \cdot p\left(x_n;\ \mu_i^{(k)},\ \sigma_i^{(k)}\right)}{\sum_{m=1}^{K} P_i^{(k)} \cdot p\left(x_n;\ \mu_i^{(k)},\ \sigma_i^{(k)}\right)}$$

This is the actual computation performed in the E step. The rest of the "construction" of the bound $b_k(\Theta)$ is theoretical, and uses Jensen's inequality to bound the logarithm $\lambda(\mathbf{X};\ \Theta)$ of the likelihood function in the following.

In summary, given an initial estimate $P_i^{(0)}$, $\mu_i^{(0)}$ and $\sigma_i^{(0)}$, EM iterates the following computations until convergence to a local maximum of the likelihood function:

E Step:

$$P^{(k)}(i \mid n) = \frac{P_i^{(k)} \cdot p\left(x_n;\ \mu_i^{(k)},\ \sigma_i^{(k)}\right)}{\sum_{m=1}^{K} P_i^{(k)} \cdot p\left(x_n;\ \mu_i^{(k)},\ \sigma_i^{(k)}\right)}$$

M Step:

$$\mu_i^{(k+1)} = \frac{\sum_{n=1}^{N} P^{(k)}(i \mid n) \cdot x_n}{\sum_{n=1}^{N} P^{(k)}(i \mid n)} \qquad \sigma_i^{(k+1)} = \sqrt{\frac{1}{d} \cdot \frac{\sum_{n=1}^{N} P^{(k)}(i \mid n) \cdot \left\| x_n - \mu_i^{(k+1)} \right\|^2}{\sum_{n=1}^{N} P^{(k)}(i \mid n)}} \qquad P_i^{(k+1)} = \frac{1}{N} \sum_{n=1}^{N} P^{(k)}(i \mid n)$$

3.3.3 Voxel classification with the EM GMM segmentation

For our specific vessel segmentation case, it is especially interesting to use an EM algorithm to fit a Gaussian Mixture Model (GMM) -determined by the weight P_i, the mean μ_i and the variance σ_i - to our MSCT scan voxels. A GMM is simply a probability distribution made up of linear combination of Gaussian distributions.

$$GMM(\mathbf{x}) = \sum_{i=1}^{k} \alpha_i G\left(\mathbf{x} \middle| \boldsymbol{\mu}_i, \boldsymbol{\Sigma}_i\right)$$

where $G\left(\mathbf{x} \middle| \boldsymbol{\mu}, \boldsymbol{\Sigma}\right)$ is a multivariate Gaussian distribution

$$G\left(\mathbf{x}\middle|\boldsymbol{\mu},\boldsymbol{\Sigma}\right)=\frac{1}{\left(2\pi\right)^{\frac{d}{2}}\left|\boldsymbol{\Sigma}\right|^{\frac{1}{2}}}\exp\left[\frac{1}{2}\left(\mathbf{x}-\boldsymbol{\mu}\right)^{T}\boldsymbol{\Sigma}^{-1}\left(\mathbf{x}-\boldsymbol{\mu}\right)\right]$$

Since the $GMM\left(\mathbf{x}\right)$ is a probability distribution it is required that the α_i's sum to 1. For the case of data clustering, each Gaussian component corresponds to a cluster.

Unlike the single Gaussian case, no analytic ML estimation exists for a GMM. Thus, the only option is to resort to the iterative methods such as the EM algorithm. In our case, the latent variables – weight, mean, variance of each Gaussian intensity distribution for the lumen, wall and background – allows us to classify of the surrounding voxels of the lumen centerline, associating each voxels to one component or cluster they are more likely to belong to.

In the classical application of the EM algorithm to mixture models the number of components k is fixed from the beginning [27]. In our specific case, our local problem consists on estimating the Gaussian intensity probability functions for the surroundings of the vessel's path. So, as we have seen in (3.3.1), the voxels along and surrounding the vessel have three main Gaussians components, so our mixture model for the vessel has 3 Gaussian mixture components:

- Myocardium or background: lowest gray intensity range values (gray voxels)
- Artery wall: middle gray intensity range values (bright gray voxels)
- Artery lumen: highest gray intensity range values (white-gray voxels)

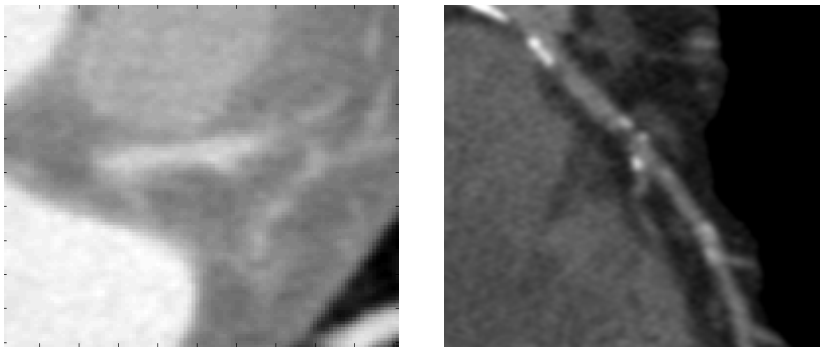

Figure 17: Two MSCT scan slice zoomed to show several arteries in the right ventricle and the different brightness level for every scan. Lumen voxels are almost white (left) and bright gray (right), myocardium voxels are gray, and wall voxels are bright gray, although hard to distinguish visually.

The algorithm is started with each component assigned an initial set of parameters that may be assigned by a human supervisor or some heuristic method or simply corresponding to random data points.

Our input data to the algorithm is the surrounding voxels of the centerline. As this method is time-consuming and the intensity values doesn't change a between consecutive tracking points $\mathbf{p}_i$ and $\mathbf{p}_{i+1}$, we use a squared prism with a cross-section width of 12 voxels per every 4 tracking steps. Results are the same than estimating the Gaussian parameters per every tracking step, but four times faster.

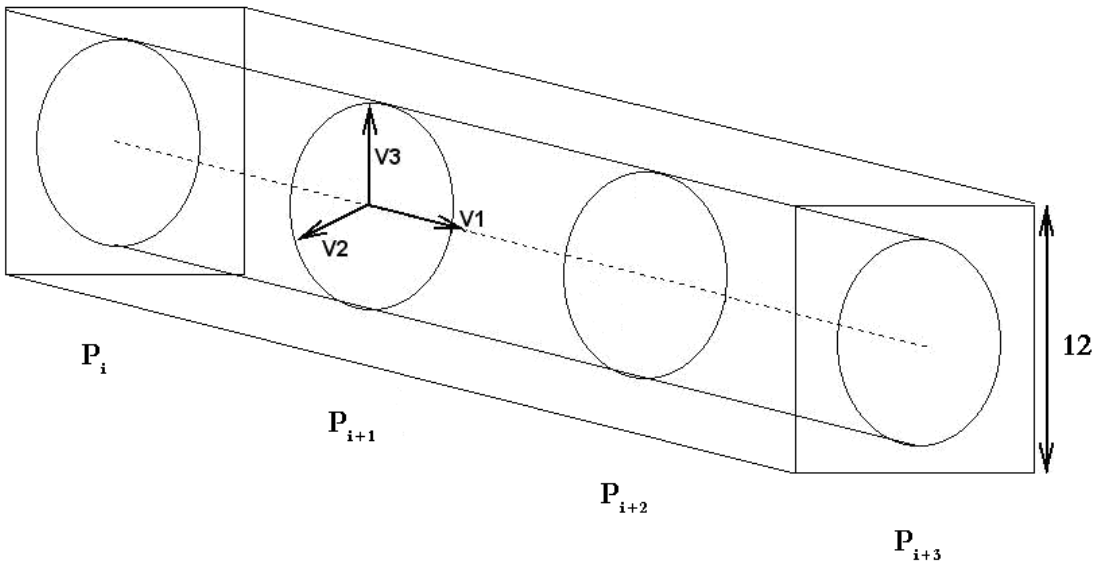

Figure 18: The EM algorithm estimates the Gaussian mixture parameters once per every 4 consecutive tracking steps for time efficiency purposes with a large input voxels selected with a square prism centered in the extracted centerline along the 4 consecutive points from $\mathbf{p}_i$ to $\mathbf{p}_{i+3}$ to have more precise GMM estimation.

The posterior probabilities for each component c and point $\mathbf{x}$ are calculated given the current GMM estimate as follows

$$p(c|\mathbf{x}) = \frac{\alpha_c G(\mathbf{x}|\boldsymbol{\mu}_c, \boldsymbol{\Sigma}_c)}{\sum_{i=1}^{k} \alpha_i G(\mathbf{x}|\boldsymbol{\mu}_i, \boldsymbol{\Sigma}_i)}$$

These posterior probabilities can be viewed as a soft classification of each centerline neighbor voxel. We associate every neighbor voxel to the intensity Gaussian range of the component c

that it is more likely to be, so the probability of being part of the component c is the maximum amongst the other two Gaussians. The mean and covariance matrices are then updated using its corresponding single Gaussian ML estimation with each point weighted by its corresponding posterior probability.

After each EM GMM estimation step for every 3 consecutive segments of the tracking (or for every 4 consecutive tracking points), we obtain 3 modeled Gaussian intensity distributions with its weight P_i, the mean μ_i and the variance σ_i (see figure 19) and we proceed to the centerline surrounding voxels classification.

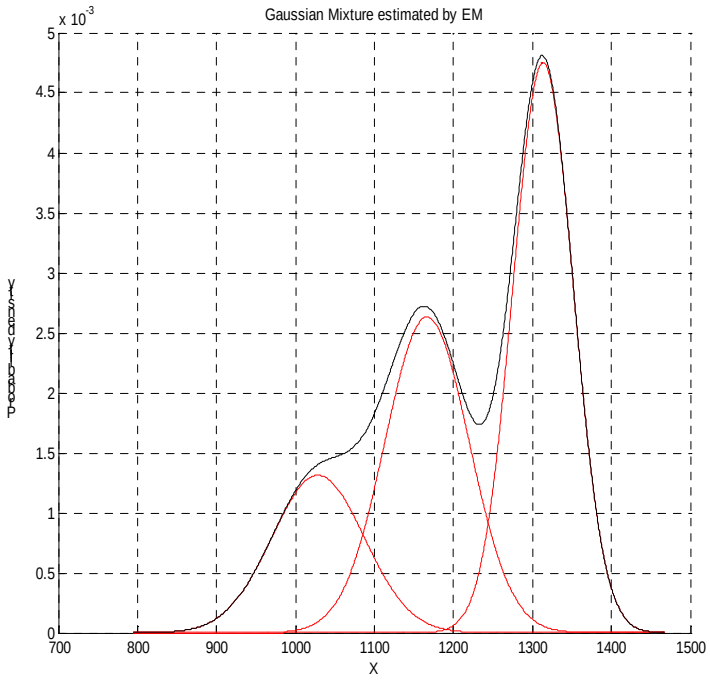

Figure 19: The EM algorithm obtains a model of 3 Gaussian intensity distribution curves, each with its intrinsic weight P_i, mean μ_i and the variation σ_i defining parameters so that they maximize the likelihood function with the true probability distribution

After the centerline's surrounding voxels classification step, we obtain an initial segmentation of the lumen and the wall.

3.4. Post-segmentation processing

The classical EM approach to mixture models has two major limitations. The first is that the number of components is fixed through out the process thus some prior knowledge of how many components are to be expected is need or an exhaustive search must be done. In our case, we have the prior knowledge of the Gaussian intensity distribution of the coronary components, so it is not a critical drawback for our method.

The second is that the EM algorithm is heavily dependant in the initial parameter estimation. The EM algorithm is efficient but excessively sensitive to the starting point (initial estimates). A poor starting point might make the EM algorithm terminate prematurely or get stuck due to computational difficulties. In our method, that involves two main practices:

- Having a large amount of input voxels to the EM algorithm so the estimated weight, mean and variance for each and every of the 3 Gaussian components are precise and reliable. Our 4 consecutive tracking point square prism allows having the *quantity* to guarantee precise EM results.

- The input voxels of the EM segmentation algorithm should contain a majority voxels form the lumen and the wall, so the following voxel classification is accurate with maximum likelihood intensity distribution estimation and distinguishes the lumen voxels from the vessel voxels with precision. Having an accurate extraction of the vessel's centerline is critical to guarantee the *quality* of the input voxels to the EM algorithm to obtain precise EM results, so the square prism should be really lumen-centered to select the maximum amount of vessel voxels and minimum amount of myocardium voxels. See figure 20 to compare the results difference.

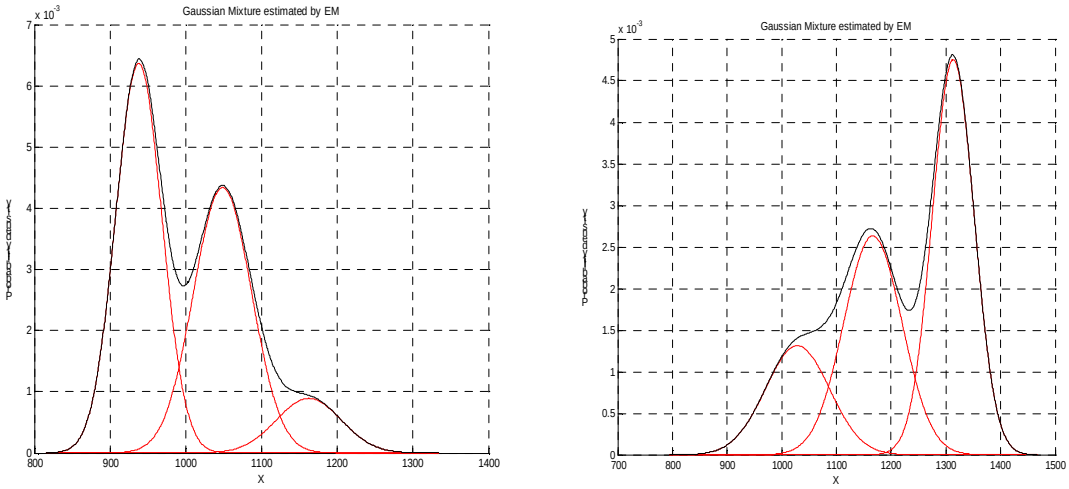

Figure 20: The EM algorithm estimation of the GMM parameters with a non accurate centerline extraction at one step segmentation (left) showing a predominant myocardium Gaussian component and residual lumen Gaussian component. With a precise centerline extraction at one segmentation step (right), the lumen and wall Gaussians have more weight and less variation, providing a much more precise voxel classification

As our initial vessel's path tracking at point 3.1 is a good approximation of the centerline, but not accurate enough (see figure 21) at every tracking step to guarantee the quality of the input voxels to the EM for GMM and assure a proper myocardium, wall and lumen classification, further practices have to be made.

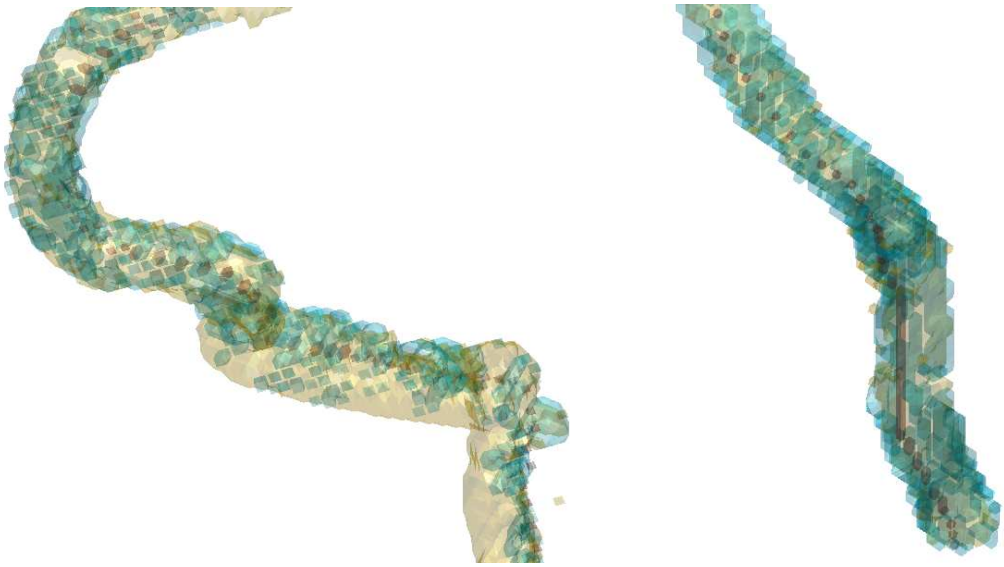

Figure 21: Two 3D views of the initial EM segmentation examples with a non accurate centerline at some segmentation steps (left: right-bottom segment; right: bottom) showing an accurate lumen but deficient wall segmentation along the artery. Morphological filtering isn't enough to compensate these low-quality results.

The analysis of this initial segmentation with the approximate Hessian centerline presents us two main conclusions: 1) The lumen segmentation is overall accurate regardless of the tracking algorithm's imprecision. 2) The wall segmentation is sensitive to the imprecision, concentrating the segmented voxels in the lopsided side of the vessel, where the centerline has deviated.

Considering this, our approach to improve and correct the initial centerline extraction to obtain an accurate and precise lumen and wall segmentation will be based on the initial lumen segmentation, and the overall segmentation method is the following:

- Perform an initial *lumen* EM GMM segmentation with the surrounding voxels of the initial Hessian centerline extraction

- Fix the initial centerline by computing the centroid of every cross-sectional lumen segmented slice of all the tracking steps

- Perform the final *lumen* and *wall* EM GMM segmentation with the surrounding voxels of the fixed Hessian centerline

3.4.1 Hessian centerline correction

To correct the initial Hessian centerline extraction, we compute the centroid of the cross-section of every tracking step by means of the $\vec{v}_2$ and $\vec{v}_3$ eigenvectors that form a base of the orthogonal plane defined by the direction vector $\vec{v}_1$.

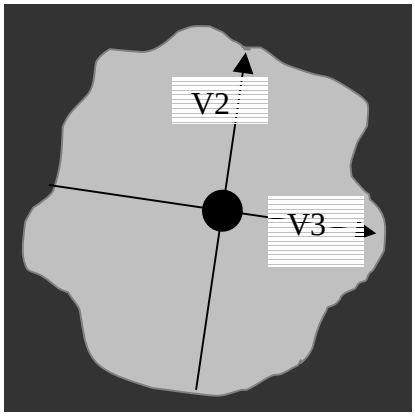

Figure 22: Orthogonal cross-section plane of the initial lumen segmentation defined by the eigenvectors $\vec{v}_2$ and $\vec{v}_3$, used to extract the centroid for every tracking step.

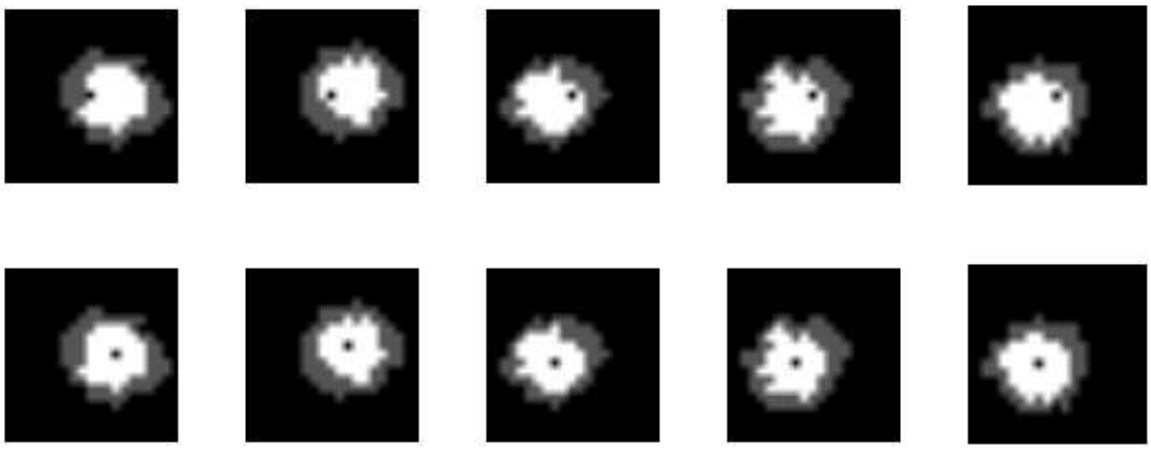

Figure 23: Orthogonal cross-section views of the lumen (white) and wall (gray) segmentation for 5 consecutive tracking steps before (top) and after (bottom) the centerline correction algorithm. The centerline point is represented by the black dot.

We obtain as well an approximate diameter of the lumen, with the diameter of a circle with the same area as the cross-section lumen slice.

The correction of the position of the centerline points implies a change for every tracking step of the direction vector $\vec{v_1}$ and the $\vec{v_2}$ and $\vec{v_3}$ vectors that form the base of the cross-sectional plane. Updating this vectors is pivotal for the further volume measurement technique.

For the direction vector $\vec{v_1}$, we update it by computing the difference between two consecutive centerline points $\mathbf{p}_i$ and $\mathbf{p}_{i+1}$:

$$\vec{v_i^1} = \overrightarrow{\mathbf{p}_{i+1}} - \vec{\mathbf{p}_i}$$

For the other two orthogonal vectors, we find them by means of a method based on the Householder reflection matrix transformation property [29]. We create a mirror vector to $\vec{v_1}$ by adding the norm $\left|\overrightarrow{v_1}\right|$ to one the vector's dimensions.

$$\vec{u} = [v_1^x + \left|\overrightarrow{v_1}\right|, v_1^y, v_1^z]$$

Afterwards, we calculate the Householder matrix with the new vector $\vec{u}$:

$$\mathbf{Q} = \mathbf{I} - 2\frac{\vec{u} \bullet \vec{u}^{T}}{\vec{u}^{T} \bullet \vec{u}}$$

This is Householder matrix or Householder reflection and the vector $\vec{u}$ is called the Householder vector. The Householder matrix **Q** is symmetric and orthogonal and reflects every vector **x** in the plane through 0 perpendicular to $\vec{u}$ as shown in Figure 24.

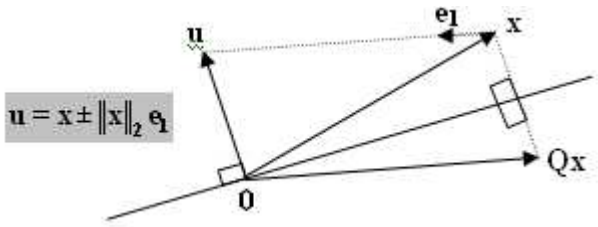

Figure 24: Householder matrix Q acting on vector x is a reflection of the vector x in a plane perpendicular to the householder vector u.

The utility of the Householder matrix for our research of the $\vec{v}_2$ and $\vec{v}_3$ vectors is that the first row of H provides us the unit vector parallel to $\vec{u}$, and the other second and third rows gives us the unit vectors orthogonal to $\vec{u}$ and orthogonal to each other. So, we obtain the desired $\vec{v}_2$ and $\vec{v}_3$ vectors.

3.4.2 Morphological filtering

Once obtaining the classification of the centerline surrounding voxels (for both segmentation steps of our method), the original segmentation of the inner and wall obtained has a good quality, but it can be improved by applying morphological filtering.

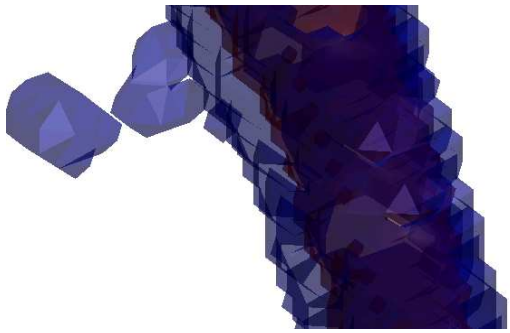

Figure 25: 3D view of the initial EM segmentation results, with presence of unconnected and parasite voxels

The first step is to perform a 3D flood-fill operation on empty voxel regions of the lumen and the wall. A 6-connected background neighbors for 3-D input is used.

The second morphological operation consists on applying image closing. The effect of this morphological operator having a small structuring element is to smooth the contours, to fuse the narrow breaks and to eliminate small holes gradually [30]. The closing of an image A by a structuring element B is defined as

$$A \bullet B = (A \oplus B) \odot B$$

Where $\oplus$ represents the dilation operation and $\odot$ the erosion operation. The former enlarges the boundaries of the planes eliminating thus the holes between them. Once the holes have disappeared, we apply image erosion to sand the volume expansion caused by the dilation. As a result, a compact segmented vessel is obtained.

The last morphological operation that is applied is the image opening. This operator smoothes the contours as it removes smaller objects than the structuring element from the surfaces of the lumen and wall.

$$A \circ B = (A \odot B) \oplus B$$

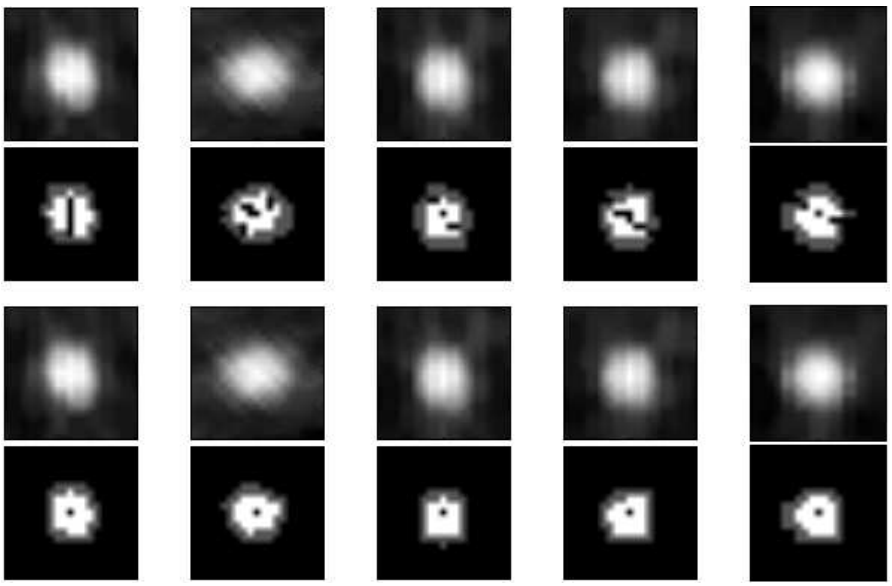

Figure 26: Comparison between the EM segmentation results for cross-section slices of 5 consecutive tracking steps with the real scan cross-section slice, before the morphological filtering (top) and after (bottom)

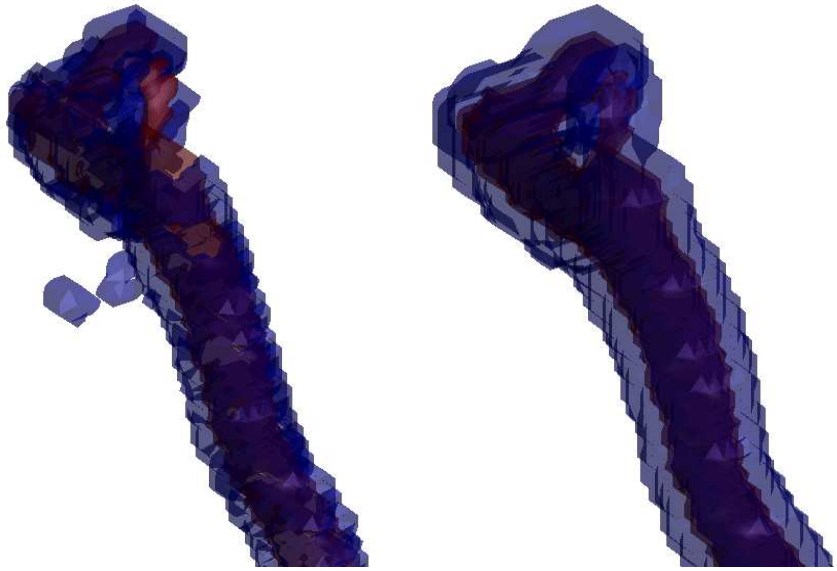

Figure 27: Two 3D view of the EM GMM segmentation results, the original segmentation with some holes and blank areas (left) and the segmentation after the morphological filtering.

3.3 Detection and Segmentation of the Soft Plaques

3.3.1 Volume estimation

At this part of this algorithm, we have an accurate centerline of the vessel, orthogonal planes to the centerline and the segmented voxels for the inner and wall of the vessel. Now we are going to extract some characteristics of the vessel in order to detect the soft plaques. Lot of papers extract the diameter of the vessel, or its mean. The problem linked to this characteristics are multiple:

- the vessel is not a perfect cylinder. So we can't define really a diameter.
- the calculus of the true centerline can take the most important time in algorithm.

That's why we are interested in a more robust feature to base our soft-plaque detection. To quantify possible narrowing of the vessel caused by plaques, we compute the effective cross-section area of the lumen. This is obtained by dividing the volume of the lumen segment between two centerline points $\mathbf{p}_i$ and $\mathbf{p}_{i+1}$ by the distance between them. We obtain the cross-

section planes with the $\overrightarrow{v_2}$ and $\overrightarrow{v_3}$ vectors computed in the point 3.4.1. Let $A_l(i)$ denote this resulting area (figure 28). In a similar fashion, we can compute the effective cross-section area of the identified arterial wall $A_w(i)$. This area measure can signal the presence of positive vessel remodeling.

$$V_{i_{normalized}} = A_i = \frac{V_i}{distance(P_i, P_{i+1})}$$

with P_i, one centerline point, and V_i the volume corresponding.

Thus, by contrasting these two area measures $A_l(i)$ and $A_w(i)$, we obtain a measure that will signal the presence of either calcified or soft plaques. Specifically, we calculate the difference between the two measures $A_d(i) = A_w(i) - A_l(i)$.

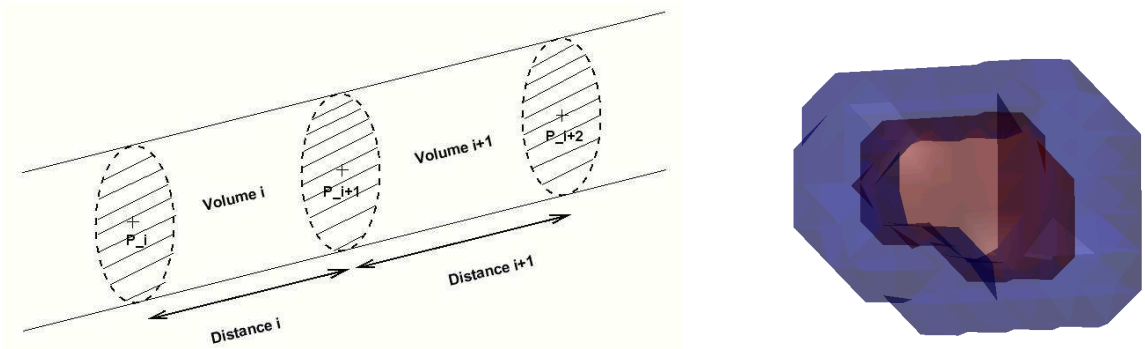

Figure 28: Two consecutive cross-section planes will establish the bounds for the local volume measurement at each tracking segment of the vessel (left). A local segment is showed (right).

The problem to segment the vulnerable plaques is that they have the same intensity's rank. So we have to have some other informations to segment them properly. Sometimes the centerline experiments sudden angle changes and, consequently, the orthogonal planes do not correspond to a transversal slice. These planes have a bigger area and create peaks in the volume plot. The segments with the beginning of a vessel ramification will give bigger areas, too. So, the problems that you can find in a vessel are:

- Bifurcations of the vessel that produces a peak in the volume curve
- A fast change in the vessel's direction (a sharp turn in the artery's path)

To avoid these peaks being considered as a soft plaque, we introduce two conditions. To minimize the bifurcations bug, we introduce threshold for the volume. To avoid having a very high peak in the volume curve, we create a sphere of radius 1.5* the estimated diameter of the lumen obtained in step 3.4.1 .

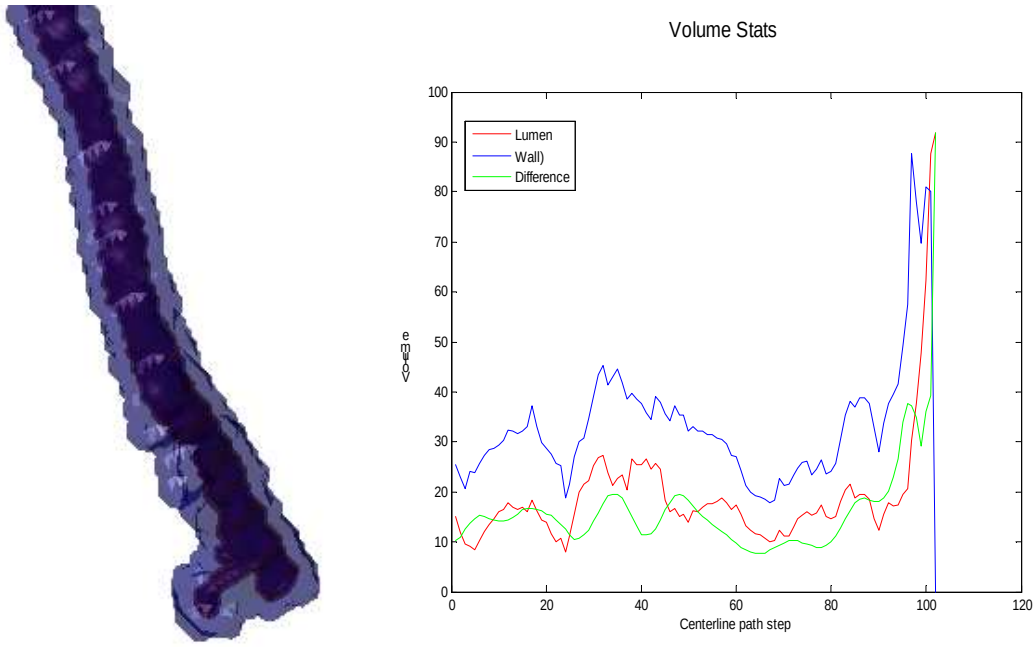

Figure 29: Example of a peak on the volume curve (right) when there is a bifurcation segmented (left).

The spherical window fixes as well the computation of far voxels not belonging to the segment of the vessel on which the algorithm is calculating the volume when the vessel present a curved path.

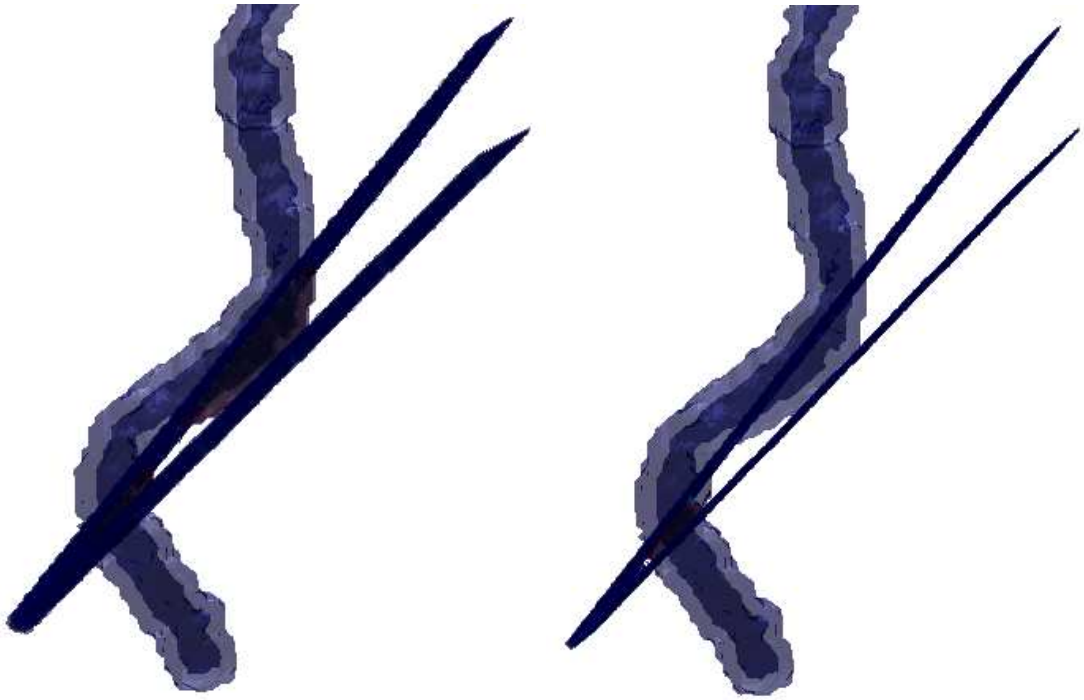

Figure 30: Example of inter-cross-section planes volume measurement in a curved artery. Without the spherical window (left), far voxels are computed producing a peak in the volume curve. Applying the window, we just compute the voxels belonging to the local segment of measurement.

To fix the problem of the fast change in the vessel in a curved segment of the coronary artery, we calculate the scalar product between two consecutive direction vectors – and normal vectors of the cross-section planes – to detect in which tracking step the vessel is curved. We compute the scalar product as follows:

$$< \overrightarrow{v^{i}_{1}} \mid \overrightarrow{v^{i+1}_{1}} >= \alpha$$

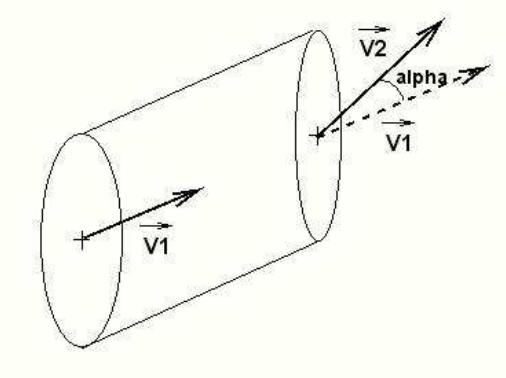

Figure 31: Coefficient α between two consecutive planes obtained by the scalar product of its normal vectors.

where < | > is the scalar product. If this coefficient is too small, the consecutive planes aren't parallel, so the amount of voxels in between the two cross-section planes can be inaccurate. Our practice to fix the inaccuracy of the algorithm for this particular case consists on modifying the cross-section plane of the tracking step $\mathbf{p}_i$ by taking a parallel plane to the next $\mathbf{p}_{i+1}$ point. Replacing the direction vector $\overrightarrow{v^i}_1$ for the $\overrightarrow{v^{i+1}}_1$ provides us a better approximation to the volume of lumen and wall voxels in between two consecutive points located in a curved segment of the artery.

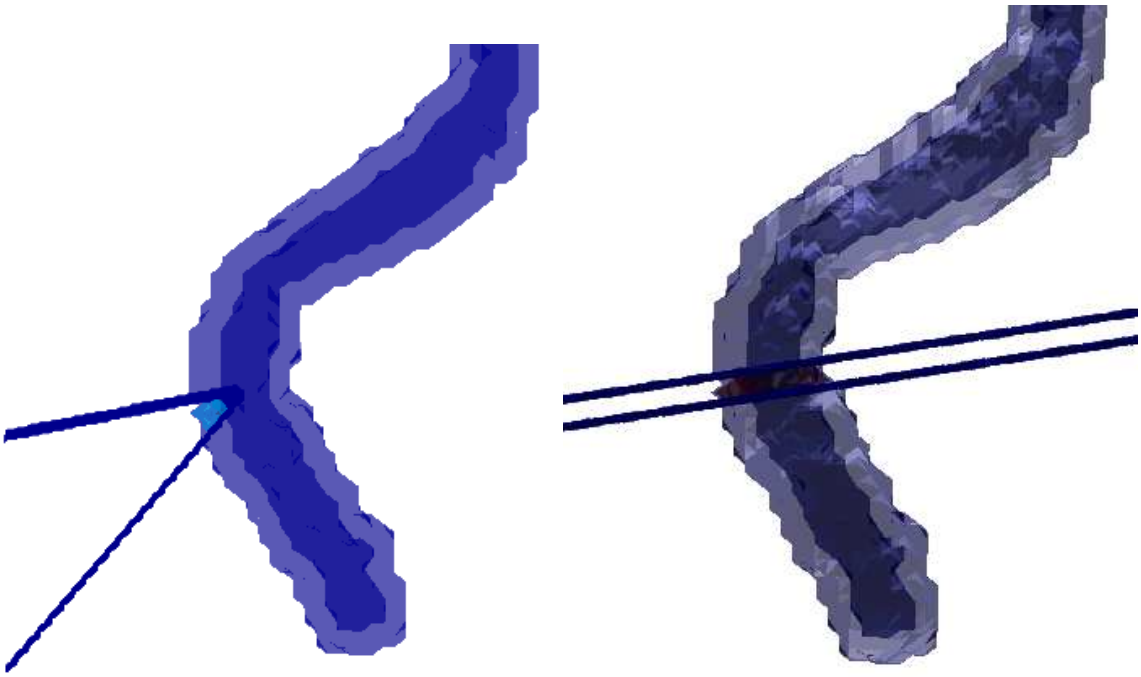

Figure 32: Correction of the first cross-sectional plane when the local segment of measurement has a curve. Consecutive planes have are not close to be parallel (left), so one of the planes is modified and becomes parallel to the other (right) in order to obtain a more accurate and precise local volume measurement.

Another solution adopted to reduce the volume estimation inaccuracy in the crooked segments of the artery is to reduce the distance between consecutive centerline tracking points. As seen in (3.1.2), the incremental gap at every tracking step is chosen to be as short as possible considering the time-cost of reducing the distance to the tracking algorithm. After analyzing the time-cost, the increment gap is almost minimum, 2 voxels.

Once we have a reliable volume curve for both the lumen and the wall, a Moving Average Filtering (MAF) with a moving window size 6 is performed in order to obtain smoother curves with less noise to make it easier to detect real drops, peaks in the volume curve so we can have a more reliable soft plaque detection. Generally speaking, there is a large class of filters that can be expressed in terms of the following moving average form,

$$y_t^T = \sum_{i=-N}^{M} w_i y_{t-i}$$

for N, M two integers and the w_i a set of weights. The simplest example is a centered moving average

$$y_t^T = \frac{1}{2K+1} \sum_{i=-K}^{K} y_{t-i}$$

The implemented MAF for our specific case quickly smoothes the input volume curve by averaging each element along with 6 samples at its sides. The elements at the ends are also averaged but the extremes are left intact. With the windows size defined this way, the filter has zero phase.

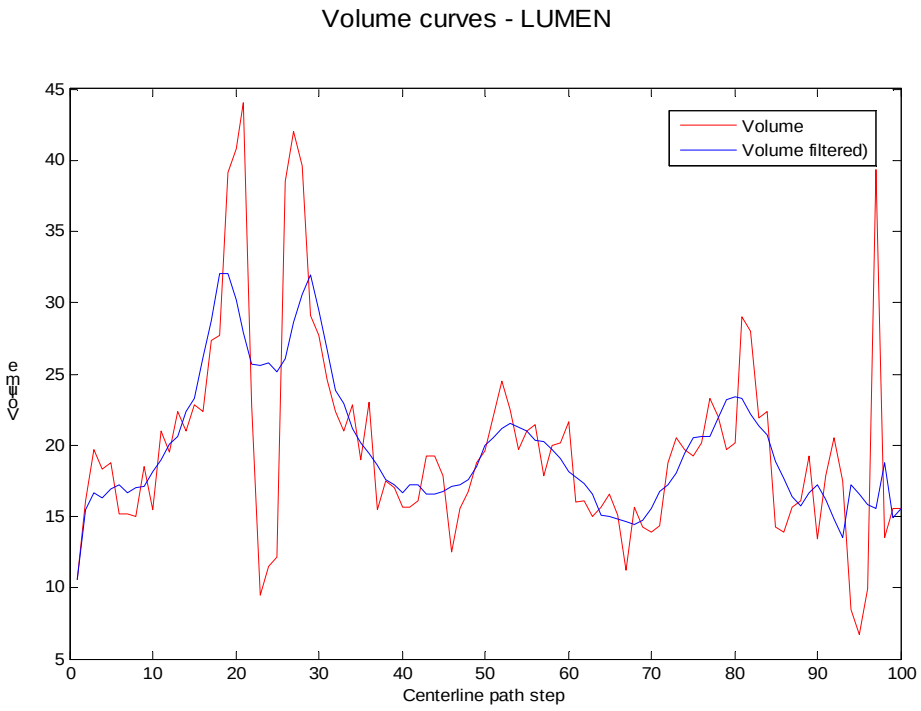

Figure 33: Original curve (in red) of the local volume at each tracking step along the vessel, and its moving average filtered version (in blue) with a smoother and less noisy plot.

This filter, acting as a high frequency barrier, eliminates the little local variations, making a mean value of its neighbors. The number of times this filtering is performed is selected by the user, being one usually enough.

3.3.2 Soft Plaque detection

Once we have a reliable and smooth volume curve, we should be able to detect the presence of soft plaques by some criteria. One interesting paper on this topic is "Using 3D Convex Hulls to Detect Coronary Artery Stenoses and Atherosclerotic Vessel Wall Lesions in Contrast Enhanced MDCT Images" [8]. They use their own convex hull algorithm to compare it to vessels and extract in this way the concavity regions. However, as they recognized, it can be only applied to a small ROI (Region Of Interest) and they mention the volume quantification as a future amelioration.

In this work, another approach is used. As before, we use the hypothesis of the slow variation of the radius along the healthy vessel (without plaques). This seems to be precise in the available artery's images. When a plaque grows in the vessel walls, it reduces its natural inner width and so it's cross-section area. The lumen volume reduction can be considered as plaque.

Recently, some studies state that the vessel may not always exhibit narrowing at soft plaque site, and it may even undergo positive remodelling [31]. This consequently poses a significant challenge for soft plaque identification in the presence of imaging noise, as a traditional approach simply based on lumen narrowing analysis no longer works well. Our goal in this work is to demonstrate the feasibility of applying image analysis on both the lumen and arterial wall for detection and quantification of soft plaques from MDCT data, and further improvements in the soft plaque detection algorithm will be required to detect this kind of plaques. Our paper is focused on the vulnerable plaques that present a narrowing in the vessel and are more likely to produce a rupture in its fibrous cap.

The goal for this detection part is to detect the local minimums of the longitudinal lumen volume curve to find the soft plaques. Once the minimums are detected, the two successive local neighbor maximums per each minimum are detected. At this point, we can find local parasite maximums in the volume curve still after the moving average filtering, by means of

thresholds we are able to ignore them. With the apriori knowledge of the size of a vulnerable plaque, thresholds for the minimum and maximum width and height of the volume curve hole are established. This threshold will mark the sensitivity of the detection and it can be selected by the user. Finally, we analyze the difference local volume curve between the lumen and the wall of the artery to classify the hole as a sudden narrowing of the inner or as a soft plaque. As the cross-section area of the wall is expected to be higher than the lumen's, having a peak in the difference curve (moving averag filtered) satisfying again the soft plaque's size thresholds condition will confirm the presence of a plaque.

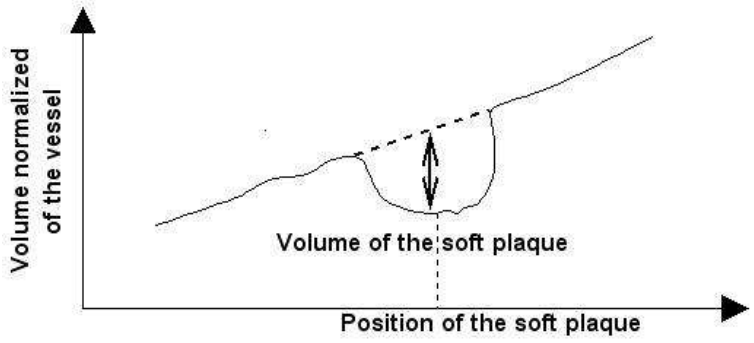

Figure 34: Operating diagram for the volume's vessel

We can implement an algorithm using convex properties to have an approximation of the volume of these soft plaques (see table 1). Based on this, our method calculates the volume that the affected region would have had in normal conditions, with a convhull method, to quantify the size of the soft plaque hole in the lumen volume curve.

We assume that the local wall volume is always higher than the lumen's. Considering this, the algorithm is as follows:

Table 1: Soft Plaque detection algorithm

```
Detect all the minimums on the lumen local volume curve
For every minimum detected
        Detect the neighbor maximums ignoring parasite maximums
        If the width (separation between maximums) and the depth of the hole > thresholds
                If the difference volume curve has a peak in the region of interest
                        Soft Plaque detected and its size is quantified
                End
        End
End
```

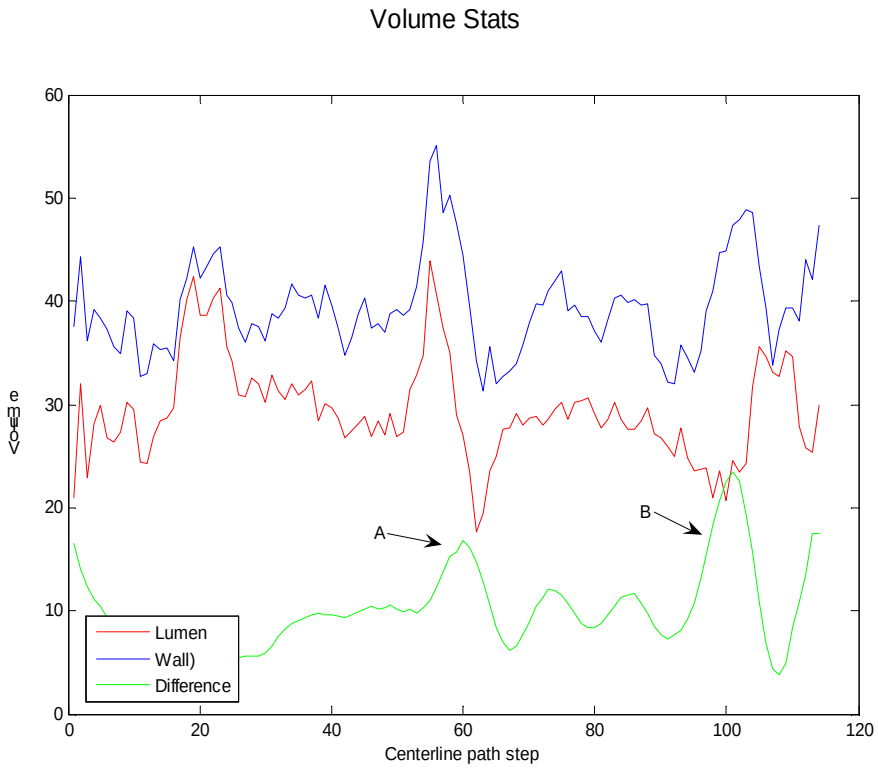

Figure 35: Local volume curves along the vessel for the lumen, wall and difference curve. A) Valley of sufficient width and depth in the lumen plot and peak in the difference plot, a soft plaque is detected. B) Peak in the difference curve but the lumen has average values; an increase of the wall's volume could be a soft plaque, but as ther is no narrowing of the inner vessel, it is not detected.

The last step soft plaque segmentation in order to show its location in the 3D rendering of the vessel, we make a simple region growing process in the region where the volume hole is. The intensity threshold for this region growing process is established with the knowledge acquired on the EM GMM estimated parameters, concretely with the mean μ_i and the variance σ_i associated to the Gaussian components of the lumen and the wall..

The method described above was tested with several datasets to assess its capacity and accuracy in the soft plaque detection and quantification. All the tests were coded and run in Matlab 7.0 (R14) with the Image Processing Toolbox, in a Hewlett Packard computer with 1.99 GHz AMD Turion 64 Mobile processor and 1GB of RAM.

The 2D real images were obtained from the Rush Hospital with a Phillips Brilliance 64-slice scanner. The algorithm had worked for every dataset, regardless of the brightness and noise level of the MSCT scan images. The following figures correspond to the execution of the algorithm when picking the seed point from the Right Anterior Descending coronary artery:

Figure 36: Initial Hessian centerline extraction

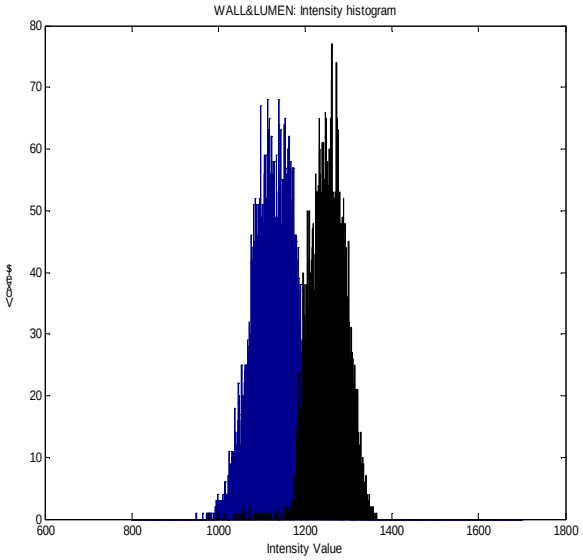

Figure 37: Intensity histogram for the wall (blue) and lumen (black)

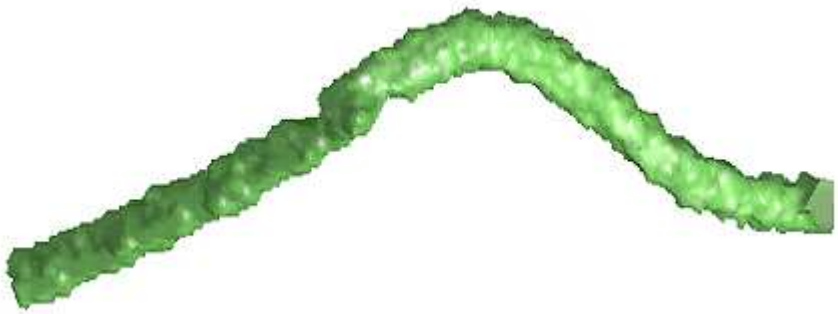

Figure 38: First lumen segmentation with an approximate centerline

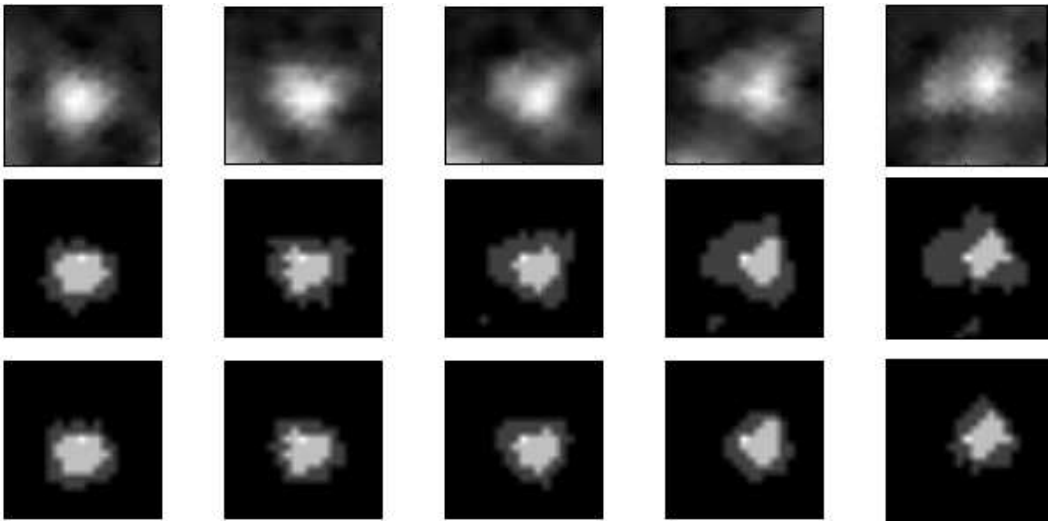

Figure 39: Cross-section views of the scan image (top), the final EM segmentation before the post-morphological operation (middle) and after the morphological filtering

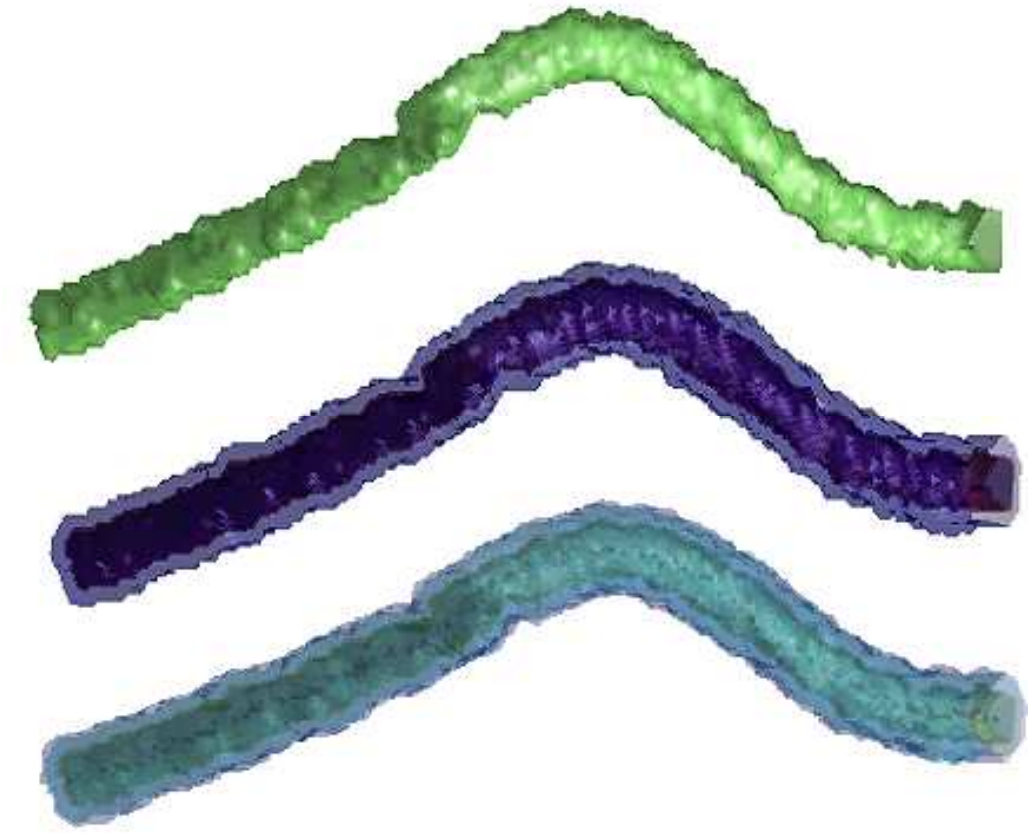

Figure 40: 3D views of the final EM segmentation results with a corrected centerline (bottom), wall and lumen segmentation (middle) and lumen segmentation (top). It is visually feasible to detect a soft plaque at the beginning of the curvature in the middle of the artery.

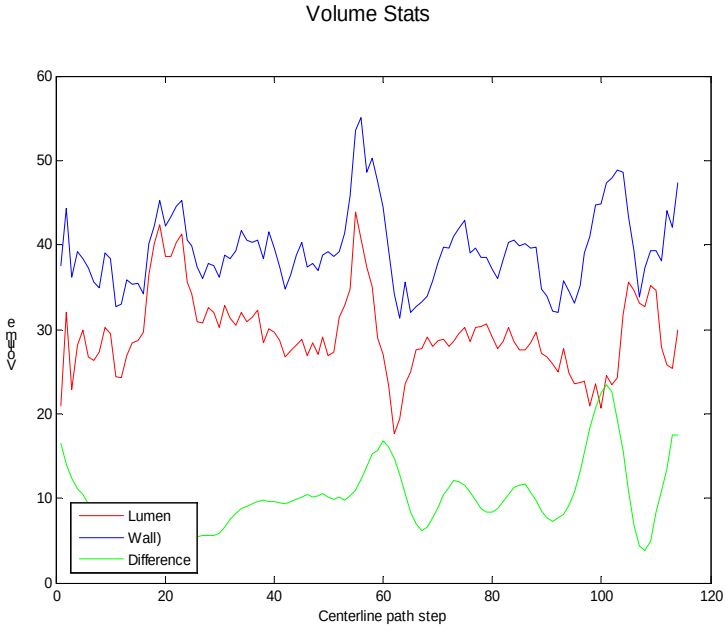

Figure 411: Volume curves along the vessel. At position 62, there is a soft plaque.

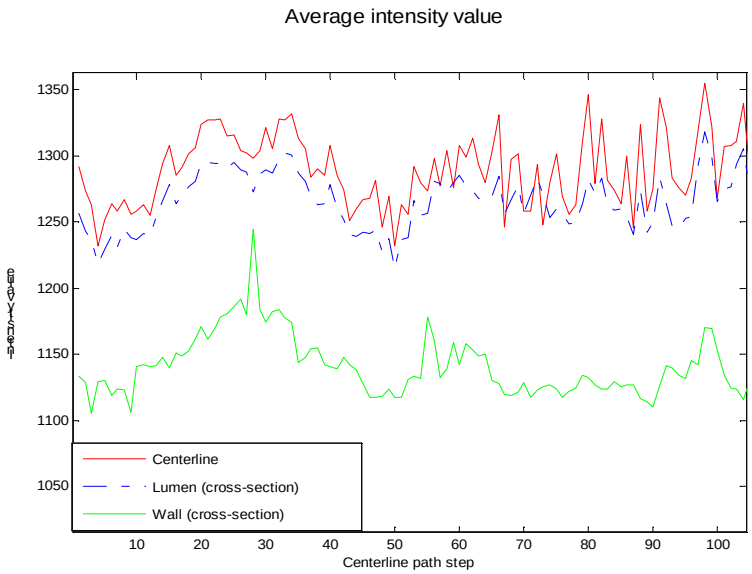

Figure 422: Average intensity values along the vessel of the centerline (the brightest, in red), the lumen (slightly darker than the centerline, in blue) and the wall (much darker than the lumen, in green)

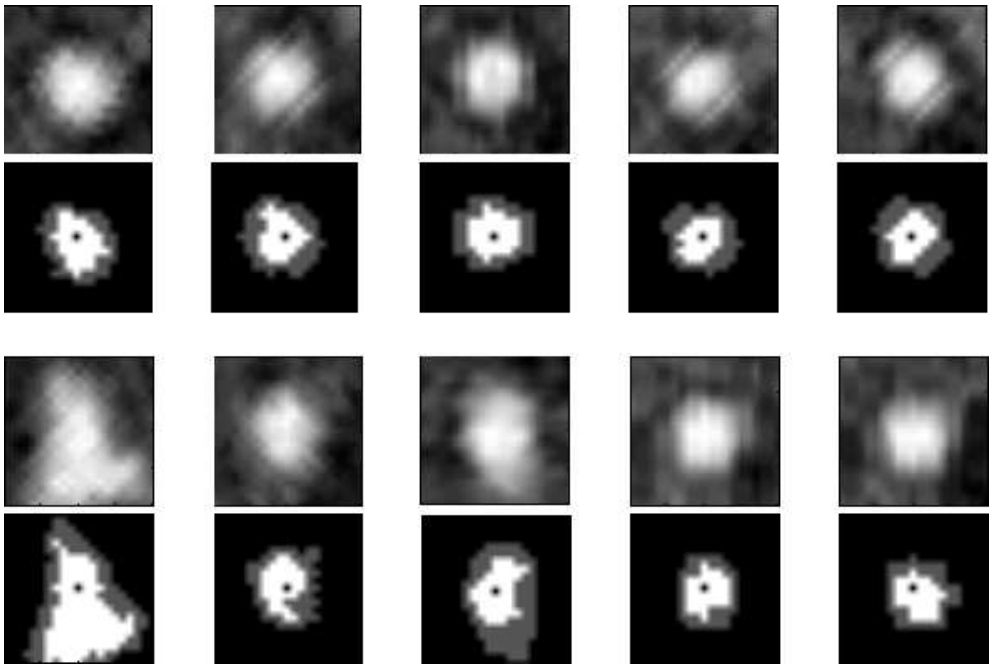

Figure 43: Cross-section views of 10 consecutives steps around the soft plaque, with real scan images on top and the segmentation on the bottom. Soft plaque is visible at steps 7 and 8. The centerline is the real centroid.

The log for the execution of the algorithm is:

***** Soft-Plaque Detection Results *****

Number of Soft-Plaques Detected: 1

- Soft-Plaque #1: Volume: 104 Tracking Step: 62

***** Average intensity *****

Centerline: 1290; Lumen: 1255; Wall: 1141

***** Computation Stats *****

Patient ID: s | Slices loaded: 139 (#110-249) | Tracking steps: 115

-Loading scan data:	44 seconds
-Initial Tracking Vessel Path:	86 seconds
-1st Lumen Segmentation & Lumen Centerline:	480 seconds
-2nd Lumen & Wall Segmentation:	439 seconds
-Lumen & Wall Volume computation:	4 seconds
-Soft-Plaque Segmentation:	18 seconds
-Printing results:	14 seconds
-1st Segmentation cost per tracking step:	4 seconds
-2nd Segmentation cost per tracking step:	3 seconds
Total Time:	1091 seconds

The EM GMM segmentation is computationally expensive, monopolizing with the 84% of the overall running time. For every tracking step, it takes 4 and 3 seconds, but it is not exactly accurate to conclude this as we perform a EM Gaussian parameters estimation per each 4 consecutive centerline points. The initial Hessian centerline extraction represents de 8% of the total time requirement.

5.4 Discussion

The present project describes a semi-automatic operative method to detect soft plaques and estimate their volume. The implementation combines techniques that have become successful in other segmentation processes, but performs its task in a slow way due to the computationally-expensive EM for Gaussian mixture model. It provides an accurate

segmentation base that will allow further development on the detection of plaque. One possible direction of future research could solve the user dependency, generating a method independent of the user's selection points and, thus, providing a fully automatic method. Knowing the geometric properties of the aorta, with its big and circle shape in the MSCTA scan, we could start tracking the whole vessel tree.

The centerline extraction method is accurate but low-efficient, further work should be done to track the centerline to avoid a second EM segmentation step that makes the current algorithm slow. The 4 tracking step window method used to input the voxels for the EM algorithm could be optimized by overlapping the windows. Using previous parameter estimations, already computed, for next EM estimations could save a lot of computation cost. As the accuracy of the volume vessel relies in the exact segmentation, any improvement in this area will ameliorate the outcome.

The soft plaque detection can be polished and, should detect all kinds of vulnerable plaques, and not only the unstable type. In addition, a soft plaque index reflecting the extent of atheroma deposits in the walls of coronary arteries could be created, emulating the works in calcium score. The present method should be clinically validated by a radiologist. Finally, when the soft plaque detection is accurate and precise and the method time-efficient, the tracking algorithm should be extended to the ramifications by detecting the artery bifurcations, so the method would be intensive and exhaustive.

BIBLIOGRAPHY

[1] Anderson, Robert N. et al., Deaths: Leading Causes for 2002. National Vital Statistics Reports, 2005.

[2] Leal, José et al., Economic burden of cardiovascular diseases in the enlarged European Union. European Heart Journal, 2005.

[3] Article from Wikipedia.

[4] Naghavi, Morteza et al., New Developments in the Detection of Vulnerable Plaque, Current Atherosclerosis Reports 2001.

[5] Indrajit et al., Multislice CT: A Quantum Leap in Whole Body Imaging, Ind J Radiol Imag, 2004.

[6] Schroeder et al., Noninvasive Detection and Evaluation of Atherosclerotic Coronary Plaques With Multislice Computed Tomography, American College of Cardiology, 2001.

[7] Gersh, Multislice Computed Tomography to Detect Atherosclerosis Regression, American College of Cardiology, 2005.

[8] Hans et al., Using 3D Convex Hulls to Detect Coronary Artery Stenoses and Atherosclerotic Vessel Wall Lesions in Contrast Enhanced MDCT Images, Harvard Medical School, 2004.

[9] Kirbas et al., A Review of Vessel Extraction Techniques and Algorithms, ACM Computing Surveys, 2004.

[10] Yan et al., Extraction of Blood Vessel in CT angiography image aided by fuzzy logic, Himeji Institute of Technology, 2000.

[11] Higgins et al., System for Analyzing High-Resolution Three-Dimensional Coronary Angiograms, IEEE Transactions on Medical Imaging, Vol. 15, No. 3, 1996.

[12] Budoff MJ. Prevalence of soft plaque detection with computed tomography, Journal of the American College of Cardiology. 2006.

[13] Leber AW, Knez A, Becker A, et al. Accuracy of MSCT in identifying and differentiating the composition of coronary atherosclerotic plaques: a comparative study with intracoronary ultrasound, Journal of the American College of Cardiology, 2004.

[14] Satyarthi et al., Gaussian Intensity Distribution Modelling of Blood Vessels in Fundus Images, IEEE Indicon 2005 Conference, Chennai, India, 2005

[15] Li et al., A Piecewise Gaussian Model for Profiling and Differentiating Retinal Vessels, ACM Computing Surveys, 2004.

[16] Yang et al., Knowledge-Based 3D Segmentation and Reconstruction of Coronary Arteries Using CT Images, Proceedings of the 26th Annual International Conference of the IEEE EMBS, 2004.

[17] Yang et al., Harmonic Skeleton Guided Evaluation of Stenoses in Human Coronary Arteries

[18] Yang et al., http://wiki.na-mic.org/Wiki/index.php/Projects:BloodVesselSegmentation

[19] Bodak et al., An improved model-based vessel tracking algorithm with application to Computed Tomography Angiography, Journal of Biocybernetics and Biomedical Engineering, 3(1), pp.41-64, 2003.

[20] Frangi et al., Model-based quantification of 3-D Magnetic Resonance Angiographic Images, IEEE Transaction on Medical Imaging, 18(10), pp. 946-956, 1999.

[21] Yan et al., Extraction of Blood Vessel in CT angiography image aided by fuzzy logic, Himeji Institute of Technology, 2000.

[22] Pock T.G, Robust Segmentation of Tubular Structures in 3D Volume DataMaster thesis, Institut fur Maschinelles Sehen und Darstellen Technische Universitat

[23] Hyeong-Seok Yu and Jun-Dong Cho, A Fast Sorting Algorithm for General-Purpose Standard Median Filter*s* in VLS Implementation, ASIC/SOC, Sep. 1999.

[24] M. Karaman, L. Onural, and A. Atalar, Design and implementation of a general-purpose median filter unit in CMOS VLSI, IEEE J. Solid-State Circuits*,* vol. 25, pp. 505-512, 1990.

[25] Dempster, A., Laird, N., and Rubin, D., Maximum likelihood from incomplete data via the EM algorithm, J. Roy. Stat. Soc. 39, pp. 1-38, 1977.

[26] T. Schneider, Analysis of incomplete climate data: Estimation of mean values and covariance matrices and imputation of missing values. Journal of Climate*,* pp. 853–871, 2001

[27] Jeff A. Bilmes. "A Gentle Tutorial of the EM Algorithm and its Application to Parameter Estimation for Gaussian Mixture and Hidden Markov Models" U.C. Berkeley TR-97-02. April 1998.

[28] Tomasi, C., Estimating Gaussian Mixture Densities with EM – A Tutorial, Duke University, 2005

[29] John Kerl, The Householder transformation in numerical linear álgebra, pp. 11-15, February 2008.

[30] P.Maragos, "Morphological Filtering for Image Enhancement and Feature Detection", in The Image and Video Processing Handbook, 2nd Edition, Elsevier Academic Press, pp.135-156, 2005.

[31] M. Madjid, A. Zarrabi, *et al.*, "Finding vulnerable atherosclerotic plaques: Is it worth the effort?" Arteriosclerosis Thrombosis and Vascular Biology, vol. 24, pp.1775-1782, 2004.